University of Crete
Department of Computer Science

Power Control-based Design Considerations for Ad hoc and Mesh Networking

Ph.D. Dissertation

Vangelis Angelakis

Advisor

Prof. Apostolos Traganitis

University of Maryland
Institute for Systems
Research

FO.R.T.H.
Institute of
Computer Science

Heraklion, April 2008

ABSTRACT

We investigate three topics that impact on the design of ad hoc and mesh networks: the properties of transmission powers assigned by a power control scheme, adjacent channel interference modeling and mitigation, and algorithms for efficient guaranteed maximal transmitter-receiver matching discovery.

Effective power control, interference mitigation and the availability of maximal matchings for use in scheduling, are network functions that take place in the two lowest layers of the OSI model. On the other hand they have a strong effect on higher layers, affecting routing, throughput and delays and thus they are all of great importance in designing ad hoc and mesh networks.

We therefore examine using analytical models and simulations how low-layer wireless network parameters such as network density and wireless environment variables, such as the path loss exponent, can affect the power assignment to the transmitters and the feasibility of matchings, under the Signal to interference-plus-noise (SINR) criterion for data reception. We devise a hypothetical application scenario, to examine how malicious jamming nodes can harm an ad hoc network, and whether the network can mitigate these jamming attempts, by simply adapting its transmitting powers.

We further introduce, a model for the calculation of the interference power in partially overlapping channels. We combine it with the SINR criterion for data reception to quantify the effect of Adjacent Channel Interference (ACI) in 802.11a, where adjacent channels are widely assumed to be orthogonal. We validate our theoretical model by applying it to a laboratory testbed,

that emulates the wireless channel and establish that in 802.11a immediately adjacent channels and next-to-adjacent channels have the potential to interfere with each other. Our experimental setup was capable to isolate the mechanisms with which the neighboring channel interference affects the 802.11a: the packet capture at the receiver and the Clear Channel Assessment (CCA) mechanism. Through experimentation we quantify the effect of ACI on throughput for both of the mechanisms above. We finally establish a link budgeting tool that accounts for ACI and directional antennas and indicate how to use it to mitigate ACI on a multi-radio mesh node.

Finally taking advantage of previous observations for the feasibility of matchings we introduce two algorithms that are guaranteed to find a maximal matching with significant efficiency in operations compared to the brute-force method.

In the course of our investigations we identified and experimentally verified mathematical conjectures of structural nature for the power assignments methods used. Their proof is left as an open challenge for the scientific (mainly mathematical) community. Furthermore, we introduce a basic building block for a tool to optimally design multi-radio nodes for use in mesh networks. This, along with the observations and methodologies provided in this thesis can lead to the design of such a tool for production systems.

Acknowledgements

I feel the need to thank the Greek General Secretariat for Research and Technology, which provided the necessary scholarship funds for my research under the 03ΕΔ844 "Π.Ε.Ν.Ε.Δ. 2003". I also thank the Institute of Computer Science of the Foundation for Research and Technology –Hellas, for providing the necessary facilities for my research. Thanks are also owed to the Institute for Systems Research of the Clark School of Engineering of the University of Maryland, for hosting me for a four month period. Last but not least, I thank the Department of Computer Science of the University of Crete, where the first decade of my Academic life has been proudly spent…

Many people deserve my gratitude and thanks. First of them is my supervisor, professor Apostolos Traganitis whom I thank for his fatherly guidance, trust and insight. I also feel the need to thank professor Anthony Ephremides for the amazing experience of working with him in ISR-UMD. Thanks are also owed to my supervising committee members: professors Vasilios Siris and Panos Tsakalides for their guidance and advise, as well as the examination committee members professors George Stamoulis, Leonidas Georgiadis and Maria Papadopouli, for their comments and advise on this dissertation.

Of my colleagues none other can be first than Stefanos Papadakis, who for the past 7 years became as close as a brother to me …words are not enough. Chariton Melissaris and Nick Kossifides both deserve my thanks for those sunny January weekends of 2008 we toiled together on the rooftops of

FORTH, for the outdoors experiments described in this dissertation. Kostas Bitsakos and Nick Frangiadakis were the best roommates possible in Maryland, Anna Pantelidou thank you for hooking us up, Polyvios Pratikakis I was lucky to meet you in MD since we weren't lucky to meet in our Heraklion… Manolis Genetzakis, Manolis Ntelakis, Kostas Mathioudakis and Nikos Petroulakis, I know I was hard on you guys, keep up the good work and have faith!

My friend, Spyros Lyberis, our friendship is like a single malt scotch, aging to perfection. I thank you from the bottom of my heart for being there in the best of times and in the worst of times. Dimo, George, Mike, Vangelis, Dimitra, Maria, Andreas, Lida, Odysseas, Sophia, Lena, Nick and Eva I thank you all and you all know the reason why.

Dedicated to my loving Father & Mother

Περιληψη

Στην παρούσα διατριβή μελετάμε τρία θέματα που επιδρούν στο σχεδιασμό ασύρματων αδόμητων (ad hoc) δικτύων και δικτύων πλέγματος (mesh):
α) Τις ιδιότητες των ισχύων εκπομπής που ένα σύστημα ελέγχου αποδίδει στους πομπούς των κόμβων, β) τη μοντελοποίηση και την αποφυγή παρεμβολής γειτονικού καναλιού και γ) αποδοτικούς αλγόριθμους για την εγγυημένη ανεύρεση μέγιστων συνόλων ζεύξεων ταυτόχρονης ενεργοποίησης σε μία αυθαίρετη αντιστοίχιση πομπών-δεκτών.

Ο αποδοτικός έλεγχος ισχύος, η εξάλειψη των παρεμβολών και η διαθεσιμότητα μεγάλων συνόλων ζεύξεων ταυτόχρονης ενεργοποίησης για χρήση στη χρονοδρομολόγηση είναι λειτουργίες που γίνονται στα δύο κατώτερα στρώματα του μοντέλου OSI. Οι λειτουργίες αυτές όμως επιδρούν στα ανώτερα στρώματα της αρχιτεκτονικής του δικτύου, καθώς επηρεάζουν την δρομολόγηση, την ταχύτητα ροής δεδομένων (throughput), και τις καθυστερήσεις, με αποτέλεσμα να έχουν σημαντική βαρύτητα στο σχεδιασμό των ad hoc και mesh δικτύων.

Για το λόγο αυτό ερευνούμε με βάση το κριτήριο του λόγου του λαμβανομενου σήματος προς παρεμβολή-και-θόρυβο (signal to interference-and-noise ratio: SINR) και μέσω αναλυτικών μοντέλων και προσομοιώσεων, τον τρόπο με τον οποίο παράμετροι χαμηλών επιπέδων των ασύρματων δικτύων, όπως η πυκνότητα του κόμβων του δικτύου, αλλά και παράμετροι του ασύρματου μέσου όπως ο εκθέτης απωλειών διάδοσης, επηρεάζουν τις ισχείς εκπομπής των πομπών και την δυνατότητα ταυτόχρονης ενεργοποίη-

σης πολλαπλών ζεύξεων. Παρουσιάζουμε επίσης ένα υποθετικό σενάριο όπου μελετάμε πώς κακόβουλοι κόμβοι (jammers) μπορούν με ελάχιστη ισχύ παρεμβολής να βλάψουν ένα ad hoc δίκτυο και κατά πόσο αυτό μπορεί να αντισταθμίσει τις απόπειρες τους απλά προσαρμόζοντας τις ισχείς εκπομπής των πομπών του.

Ακόμη, ορίζουμε ένα μοντέλο για τον υπολογισμό της ισχύος της παρεμβολής που δημιουργείται από μερικώς αλληλοεπικαλυπτόμενα κανάλια. Το συνδυάζουμε με το κριτήριο του SINR για να ποσοτικοποιήσουμε τα αποτελέσματα της παρεμβολής γειτονικού καναλιού (adjacent channel interference: ACI) στο 802.11a, όπου ενώ τα γειτονικά κανάλια θεωρούνται ευρέως ως ορθογώνια δείχνουμε ότι όχι μόνο το άμεσα γειτονικό, αλλά και το επόμενο του έχουν την δυνατότητα να δημιουργήσουν παρεμβολές σε ένα κανάλι. Επιβεβαιώσαμε το θεωρητικό μοντέλο εφαρμόζοντας το σε εργαστηριακή πλατφόρμα (testbed) στην οποία το ασύρματο κανάλι εξομοιώνεται από καλώδια, εξασθενητές, διακλαδωτές και αθροιστές. Η πειραματική μας διάταξη σχεδιάστηκε ώστε να έχει την δυνατότητα να απομονώνει τους μηχανισμούς του 802.11a που επηρεάζονται από τις παρεμβολές: την λήψη δεδομένων στον δέκτη και την εκτίμηση ελεύθερου καναλιού (clear channel assessment: CCA). Μέσω πειραμάτων προσδιορίσαμε ποσοτικά την επίδραση της ACI στο ωφέλιμο throughput για καθένα από τους δύο μηχανισμούς. Επίσης, ορίσαμε ένα εργαλείο για τον προϋπολογισμό της ισχύος παρεμβολής, που λαμβάνει υπόψη την ACI και την χρήση κατευθυντικών κεραιών. Δείχνουμε με μια πλατφόρμα εξωτερικού χώρου στο πραγματικό ασύρματο μέσο, πώς μπορεί αυτό να χρησιμοποιηθεί για ένα κόμβο ασύρματου mesh δικτύου με πολλαπλές διεπαφές.

Τέλος, έχοντας ως οδηγό τις αρχικές παρατηρήσεις μας για την δυνατότητα ταυτόχρονης ενεργοποίησης πολλαπλών ζεύξεων, κατασκευάσαμε δύο αλγόριθμους που εγγυώνται την εύρεση μέγιστων συνόλων εφικτών αντιστοιχίσεων και έχουν σημαντικά βελτιωμένη απόδοση σε σχέση με την μέθοδο brute-force.

Κατά την πορεία της ερευνάς μας επιβεβαιώσαμε μέσω προσομοιώσεων δομικές μαθηματικές εικασίες που έχουν εφαρμογή στις μεθόδους ανάθεσης ισχύος που χρησιμοποιήσαμε. Η απόδειξη τους μένει ανοιχτή πρόκληση για την επιστημονική (κυρίως μαθηματική) κοινότητα. Επίσης, στην εργασία αυτή παραθέτουμε το θεμελιώδες στοιχείο για ένα εργαλείο βέλτιστου σχεδιασμού κόμβων πολλαπλών ράδιο-διεπαφών για χρήση σε mesh δίκτυα. Σε συνδυασμό με τις παρατηρήσεις και τις μεθοδολογίες που υπάρχουν σε αυτή τη διατριβή, ανοίγεται η δυνατότητα κατασκευής ενός εργαλείου για χρήση σε πραγματικά συστήματα.

TABLE OF CONTENTS

List of Figures

List of Tables & Algorithms

1
INTRODUCTION

This dissertation investigates three topics that reflect in the design of ad hoc and mesh networks: the properties of transmission powers assigned by a power control scheme, adjacent channel interference modeling and mitigation, and designing algorithms for efficient guaranteed maximal matching discovery.

Wireless Ad hoc networks are collections of possibly mobile nodes communicating over the wireless medium. These nodes can dynamically self-organize into autonomous, unplanned, arbitrary and temporary topologies, allowing devices to exchange information, without the central arbitration of a Base Station or an Access Point. The basic ad hoc network is a peer-to-peer network formed by a set of wireless nodes within the range of each other that set up a temporary single-hop ad hoc network. The communication limitations of this architecture are overcome by the multi-hop ad hoc paradigm. With it, the users' devices make up a network that cooperatively provides routing functionalities. Neighboring nodes exchange information directly, while distant devices achieve end-to-end communication by forwarding their data over intermediate nodes of the network.

Mesh networks, in the past few years, evolved as the commodity outlet of the vast research investment in ad hoc networking of the previous decades. They have all the requirements of multi-hop ad hoc networking, with the added value and benefits of supporting connections to a wired infrastructure. Although mesh network architectures can be far more elaborate than the one of the multi-hop ad

hoc paradigm, the mesh nodes that are required to perform the key routing functions, are typically not considered to be constrained in size, or computational and energy efficiency and can be equipped with directional antennas.

The power control problem in wireless ad hoc and mesh networks is that of selecting transmission powers at each radio interface in the network, for a given time-scale which can range from a per-packet assignment to a static, once-and-for-all assignment. The key difference of applying power control to ad hoc versus infrastructure wireless networks is that in the latter there is a centralized authority with more capabilities and information than the rest of the nodes which can arbitrate the process, while in the former, power control has to be applied in a distributed fashion. The problem is therefore complex, but is also important since the choice of the transmission power values fundamentally affects many aspects of the operation of the network, since it determines:

i) the quality of the signal arriving at a receiver
ii) the effective range of a transmission
iii) the amount of the interference it creates for the other receivers

Because of these factors, power control affects the physical layer due to (i), the Medium Access sub-layer, due to (ii)&(iii), the Network layer, since (ii) affects the network connectivity and topology and hence routing, and finally the Transport layer as the effects of interference, as we shall see in this dissertation can cause increased bit-error rate leading to packet drops, similarly to congestion.

Therefore the problem of transmission power control is an exemplary cross-layer design problem; affecting all layers of the OSI protocol stack from physical to transport, and affecting key performance measures, including throughput, delay and energy consumption. Assigning optimal transmission powers with an intelligent fashion and using adaptive power control in a single-channel ad hoc wireless network allows wireless devices to set up and maintain

communication links with minimum power, while satisfying quality of service (QoS) constraints.

Such constraints can be modeled as Signal to Noise-plus-Interference (SINR) thresholds that must be exceeded at each receiver. These thresholds will depend on:

i) the modulation and coding scheme, affecting the transmission rate and
ii) the bit error rate (BER), which in conjunction with the transmission rate affects the effective throughput.

Similarly, in multi-radio, multi-channel mesh systems, using channels that partially overlap, power control is used in order to effectively mitigate the ACI which on such a mesh system node cause for significant performance degradation.

Benefits of an optimal power assignment scheme are not limited to the achievement of communication with the desired QoS parameters. Using the minimum powers to achieve the communication goals results also to increased energy efficiency and in the case of mobile battery-operated devices, longer network lifetime. Finally, the resulting interference reduction increases the overall network capacity by allowing higher frequency reuse.

RELATED PREVIOUS WORK

For a long time, power control and interference mitigation techniques were designed for wireless networks with centralized architectures. The key benefit of such architectures, is that we can rely upon a central controller, which can be assumed to have full knowledge of the channel state for all possible links in the network.

Under these assumptions for a cellular network, in [GVGZ'93] Grandhi, et.al., use the Perron-Frobenius theory and prove that using as power vector the

eigenvector associated with the largest (Perron) eigenvalue of an irreducible matrix defined by the link gains, produces the maximum, common to all receivers, Signal to Inference Ratio (SIR).

In noisy environments [PTC'05, T'05] the Perron eigenvalue is used to determine whether a given set of links, a *matching* of transmitters to receivers, can function under the SINR thresholds imposed (*feasible matching*). The actual minimum power vector is calculated as the solution of an $N \times N$ linear system. Since these two power control schemes are of fundamental importance for our work, we summarize their key points in appendix I. Foschini and Miljanic in [FM'93] introduced a distributed algorithm proven to converge to the minimum power vector that achieves the SINR constraints.

These power control schemes work for a time frame, at which the network nodes are assumed to be partitioned in two disjoint groups of transmitters and receivers. In [BE'04] Borbash and Ephremides proved that for SINR thresholds $\theta \geq 1$ one, at most, such matching is feasible for each given grouping of transmitters & receivers in the network. Having a CDMA system in mind, where θ may be assumed to take small values because of the spreading gain, the authors examine the feasibility of matchings with SINR thresholds $\theta < 1$. The existence of interesting SINR threshold values is proven and bounds are given for: a threshold $\theta_{safe}(T,R)$ that provides feasibility for all matchings in a given transmitters-receivers partition of the network nodes and a threshold $\theta_{safe}(*)$ where any matching of nodes, for any partition of the node set to transmitters-receivers in the network becomes feasible.

In mesh networking a backbone routing node, in contrast to a typical infrastructure Wireless LAN scenario, is no longer required to have its own wired connection to the wired infrastructure, but rather rely on other routing mesh nodes to forward its traffic to one that is connected to the wired backbone [AWW'05]. The

key benefit of mesh networking is the fast and inexpensive range extension of the wired network infrastructure. The major technological difference from the typical infrastructure wireless LAN is the shift from single-hop wireless networking to multi-hop wireless networking. This leads to many possible design choices for the architecture of a wireless mesh node.

The well known capacity issues from the ad hoc networking area [GK'00] and inexpensive off-the shelf wireless devices of the IEEE 802.11 letter-soup have made the multi-radio design of mesh nodes the most appealing one both for research and production. In such multi-radio designs some of the interfaces form wireless point-to-point links with neighboring nodes for backbone connectivity and some for client access. Each of the wireless interfaces of such a node can be connected to an antenna selected from wide range of characteristics, depending on the overall design of the network.

Analytical and simulation-based approaches for the evaluation of such systems have been found to be limited, due to coarse simplifications in the cross-layer modeling and the widely variant wireless channel. Also, the fast spreading of community-based mesh-based networks [SW'08, AWMN'08, HSWN'08, W'08], has driven research in this area closer to the production and analysis of real systems.

Testbed platforms and experimental measurements, in the past few years are very often used by the community, to provide more realistic performance evaluation of various networking solutions, using commercial, off-the shelf hardware and opening new areas for hypotheses testing and better understanding of production systems.

In [RPDGK'05] the authors perform one of the earliest testbed studies in the mesh networking area, being the first to report a range of issues that can be observed when experimenting with a multi-radio wireless testbed. Using 802.11b off-the-shelf Prism 2.5-based radio interfaces for their platform they investigated

the different choices one may face in the design of a multi-radio mesh node and reported that simultaneous activation of multiple radios on the same node leads to degradation in performance due to: i) board crosstalk, ii) radiation leakage, and iii) inadequate separation between antennas. During our work, reproducing their Prism 2.5 single-board multi-radio implementation we attributed most of the reported degradation in throughput to a problematic implementation of the monitoring mode on the HostAP Linux driver for WLAN Prism 2.5-based interfaces which leads to a CPU load of nearly 100% on the machine that hosts multiple monitoring interfaces. Not enabling the monitoring mode simply alleviated the reported board crosstalk issue, leaving ACI as the only source of problems, once the antennas were sufficiently separated.

The authors of [CHKV'06] move to Atheros-based 802.11a interfaces and perform testbed experiments to quantify the effect of ACI on a dual-radio multi-hop network. Their work includes both in-lab and outdoor experiments, using omni-directional antennas. The former indicated that the Atheros AR5213A-chipset interfaces they employed were indeed compliant with the spectral requirements of the 802.11a specification [802.11a'99]. Their testbed was again based on a single board Linux-based PC that hosted the two interfaces and used the MadWifi driver [M'08]. They did not report any board crosstalk and using omni-directional antennas for their outdoor testbed they were the first to suggest increasing channel separation and antenna distance as well as using directional antennas in order to mitigate the effects of 802.11a ACI, which they reported to reduce performance because on a multi-interface node the transmitter can interfere with one of its own receiving interfaces that is tuned on a different channel. These reports of 802.11a ACI came without any theoretical justification, or attempts for explanation. ACI is measured and it is established in a more robust fash-

ion than that of the previous work that 802.11a ACI exists, though they still failed to give a reason for it.

In [MSBA'06] the authors produce a simple model to theoretically quantify the ACI power leakage. Their key idea is focused on taking an integral over the whole overlapping region of the interfering channels spectral masks. They apply it to the spectral masks of 802.11b/g which have known overlap issues due to poor channelization [802.11a'99], and that of 802.16. They state that the use of partially overlapped channels is not always harmful. Furthermore they state that a careful use of some partially overlapped channels can often lead to significant improvements in spectrum utilization and application performance, with respect to the interfering nodes' distances.

The authors of [ZINK'07] conducted a measurement study to examine the performance and configuration of a multi-radio 802.11g node. Their findings verified that the placement (orientation and distance) of directional antennas on a multi-hop node have a significant impact on the achieved throughput. Part of the observed behavior was attributed to the beam patterns of the directional antennas used in the measurements. To our knowledge, this is still is the only work besides ours that attempts to quantify and explore the usage of directional antennas in a systematic fashion.

DISSERTATION ORGANIZATION & OVERVIEW

This dissertation is organized in 4 more chapters. In chapter 2, following this introduction, we present a thorough study of two well-known power assignment methods, in wireless ad hoc networks. We examine how network density and the path loss exponent, affect the power assignment to the transmitters and the feasibility of matchings. Furthermore, in a hypothetical application scenario, we examine how malicious jamming nodes can reduce the aggregate throughput of an

interference-limited network, breaking its connectivity and whether the network can mitigate these jamming attempts, by simply adapting its transmitting powers. We finally provide a strategy for a mobile jammer to optimally harm a network spending minimum transmission power.

In chapter 3, we introduce, a model we developed concurrently with [MSBA '06], for the calculation of the interference power by partially overlapping channels. We combine it with the SINR criterion for data reception to quantify the effect of ACI in 802.11a, where adjacent channels are widely assumed to be orthogonal. We validate the results from our theoretical model by applying it on a laboratory testbed, in which we use signal splitters/combiners and fixed attenuators to emulate the wireless channel and establish that in 802.11a immediately adjacent channels and next-to-adjacent channels have the potential to interfere with each other. Our experimental setup was able to isolate the mechanisms that the neighboring channel interference affects the 802.11a: the packet capture at the receiver and the Clear Channel Assessment (CCA) mechanism. Through experimentation we quantified the effect of ACI on throughput for both of the mechanisms above. Furthermore, moving to an outdoors testbed of medium range lings, we included our ACI quantification model, along with direction antenna accounting, in a link budget which could be used to predict the transmission rate in multi-radio nodes. Identifying that coupling our models with uncertain models for path loss, inaccurate device specifications provided by hardware vendors and a misreporting, open-source driver, we describe in appendix II a calibration method to be used for a production software tool which can be used to design maximum throughput achieving multi-radio nodes.

In chapter 4, we identify interrelations between super and sub sets of matchings which enable us to limit the number of operations, and more significantly limit the search space when dealing with the maximal matching problem.

We propose a simple data structure which can be built off-line for an increasing number of potential links and use it to describe our algorithms that perform significantly fewer operations than a brute-force search.

Finally, Chapter 5 concludes this dissertation, discussing the key results presented, evaluating our contribution, and pointing to unsolved problems that arose during our work, as well as to as well as to new directions to be followed.

Most of the work presented in this dissertation has already been presented in international conferences, while we are preparing journal versions of the work in chapters 2 & 3. Chapter 2 was initially presented in PIMRC'06 [EAT'06]. Our initial work on the ACI modeling was presented in the student poster competition of IEEE INFOCOM 2007 [ATS'07]. The indoors testbed results were presented at the IEEE Radio & Wireless Symposium of 2008 [APST'08], while the outdoors testbed and an initial proposal for the calibration process was given in [APKST'08] which was presented in the IEEE WiOpt adjunct workshop WINMEE 2008

.

2

SINR-BASED POWER ASSIGNMENT FOR AD HOC NETWORKS

In this chapter we present a thorough study of power assignment for wireless ad hoc networks. Specifically, we examine the well known power assignment methods [GVGZ'93, PTC'05, T'05] based on the eigenvalues of matrixes that describe the network topology and the communication quality requirements.

We investigate how a typical wireless network parameter, the network density, and an environmental variable, the path loss exponent, will affect the assignment of powers at the transmitters, and the ability to concurrently operate more than one links on the same channel. In the first part of this chapter we present some structural observations on the power assignment based on the method described. In the second part of this chapter we examine how malicious jamming nodes can reduce the aggregate throughput of an interference-limited network similar to the one presented in the first part, by breaking the connectivity of its links. We illustrate that the network cannot effectively mitigate such jamming attacks by merely adapting its transmission powers. We finally present a procedure, based on more structural observations, for a single node to optimally jam such a network spending minimum transmission power.

2.1 OBSERVATIONS ON THE POWER ASSIGNMENT

A. *MODELING, SETUP AND EXPERIMENTS*

The network we consider in this chapter is a time-slotted wireless system with $2N$ nodes. All nodes in the network share a single channel. An orthogonal low rate communication channel is assumed, to carry control, signaling and synchronization information. Each node has an omni-directional antenna, and at any given time-slot either its transmitter or its receiver is activated.

For a time-slot t we label N of the nodes as $T_1 \ldots T_N$ and the remaining N nodes as $R_1 \ldots R_N$. We assume that each node T_i, for $i = 1 \ldots N$, at the given time-slot, is transmitting to receiver R_i, forming the ***communication link*** (i, i). The set of these N links is the ***node matching*** for this time-slot. At the same time, the signals emitted from each transmitting node T_j, arrive not only at R_j, but also at any receiver node R_i $i \in [1 \ldots N] \backslash \{j\}$ with each pair forming an ***interference path*** (i, j).

We shall assume full knowledge of losses along the links of the matching and the interference paths and examine the centralized solution for a single time-slot. Since the Foschini-Miljanic distributed power control algorithm [FM'93] converges to the centralized minimum power solution of [PTC'05, T'05] the conclusions we draw apply to a distributed system as well.

In order to model the path losses we use a generalization of the free-space path loss, assuming path loss to be inversely proportional to the n-th power of the distance between transmitter and receiver. We denote as G_{ij} the loss of a signal arriving at receiver i from transmitter j and we take it to be:

$$G_{ij} = L \cdot d_{ij}^{-n} \tag{2.1}$$

where L is constant for a given setting, modeling the first meter losses and depends on the frequency of the channel at which the system operates. The ***path loss exponent n*** has typically values from 2 up to 5, depending on the environment [R'02, PK'02] and is assumed to be fixed for the duration of the time-slot for all links.

In order to transfer information at a given rate over each communication link (i, i) during a time-slot the SINR, the ratio of the received signal-of-interest power over the received aggregate power of interference plus noise, at R_i must exceed a ***threshold*** θ_i which depends on the modulation scheme, the transmission rate used and the desired bit error rate [P'95, LYCZ'06], that is:

$$\frac{P_i G_{ii}}{\sum_{j \neq i} P_j G_{ij} + \nu_i} \geq \theta_i \tag{2.2}$$

In eq.(2.2), P_i denotes the transmission power of the i-th transmitter and ν_i is the noise power at the receiver. The product $P_i G_{ii}$ is the power with which the signal of interest arrives at receiver i, while $\sum_{j \neq i} P_j G_{ij}$ is the power of the aggregate interference at receiver i. Expanding eq.(2.2) we have:

$$P_i G_{ii} \geq \theta_i \left(\sum_{j \neq i} P_j G_{ij} + \nu_i \right) \Leftrightarrow P_i \geq \left(\sum_{j \neq i} P_j \theta_i \frac{G_{ij}}{G_{ii}} + \frac{\theta_i \nu_i}{G_{ii}} \right) \Leftrightarrow P_i - \sum_{j \neq i} P_j \theta_i \frac{G_{ij}}{G_{ii}} \geq \frac{\theta_i \nu_i}{G_{ii}}$$

Now, defining u, and F as:

$$u = \left[\frac{\theta_1 \nu_1}{G_{11}}, ..., \frac{\theta_N \nu_N}{G_{NN}} \right]^T \text{ and } F = \left[F_{ij} \right] = \begin{cases} \theta_i \dfrac{G_{ij}}{G_{ii}} & \text{, for } i \neq j \\ 0 & \text{, for } i = j \end{cases} \tag{2.3}$$

we can rewrite eq.(2.2) in matrix form, and so we reduce the problem of finding powers to satisfy eq.(2.2) to finding a power vector: $P = [P_1, .., P_N]^T$ which satisfies:

$$(\mathrm{I}_N - F)\cdot P \geq u \tag{2.4}$$

Iff ρ_F, the Perron (largest) eigenvalue of F, lies inside the unit circle then the matrix $(\mathrm{I}_N - F)$ is a M-Matrix[1] [G'64, HJ'91] and as such it has an inverse which is non-negative. Therefore eq.(2.4) can then and only then be solved with a strict equality and so we obtain the minimum power vector as:

$$P^* = (\mathrm{I}_N - F)^{-1} u \tag{2.5}$$

Using this power vector, the SINR at each receiver i becomes equal to θ_i. In such a case, where $\rho_F < 1$ and so a power vector to satisfy eq.(2.2) can be found, the matching described by F and u is said to be ***feasible*** .

To study the power assignment process that was described above, we consider a single time-slot. For the duration of this slot we assume all channel gains to be constant. We consider a feasible set of links and we examine the properties of the minimum power vector.

To do this, in simulation, $2N$ nodes are placed in a circular area of radius r using a uniform random distribution for their position. The nodes are enumerated, N of them are randomly selected as receivers, the remaining N as transmitters and one of the $N!$ possible matchings is randomly picked to form the N links.

Unless noted otherwise, we assume that all receivers have an SINR threshold that equals the upper bound for $\theta_{safe}(T, R)$ given in [BE'04, B'04], that is: $\theta_i = \theta = 1/(N-1)$. This was primarily chosen in order to have more than one feasible matchings and therefore save simulation run time. Since $1/(N-1)$ is proved to be a rather loose upper bound for $\theta_{safe}(T, R)$, not all matchings produced with it were expected to be feasible and indeed this led us to examine how this bound performs in terms of matching feasibility by

[1] $(I - F)$ is a M-Matrix iff $\rho_F < 1$ since it is in the form $(k \cdot \mathrm{I} - F)$ with $\rho_F < k$ and F is a non-negative.

calculating the probability of feasibility of a random matching.

In the simulation, we consider a matching to be feasible if the Perron eigenvalue of the matrix F is inside the unit circle. If the matching is infeasible, we simply discard it and examine another one for the same node positions and node role assignment. The minimum power vector P^* satisfying eq.(2.2) is then derived by solving eq.(2.4) with a strict equation. As we take node positions and matchings at random, we run the simulation and record the P^* vector, as well as any other parameter we are interested in, over a large (typically in the order of 10^5) number of time-slots. The results we present, unless otherwise noted, are mean values over the simulation runs.

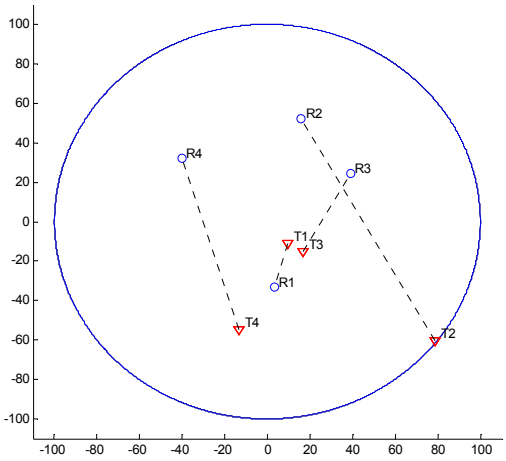

Figure 2.1: *A simulated feasible matching of 4 links in a circular area of r = 100m.*

In the process of conducting our simulation experiments to examine the SINR minimum power assignment, we observed that the SINR threshold of $\theta = 1/(N - 1)$ that we had selected, would not provide feasible matchings frequently enough. To look further into this we examined matchings of $N = 2$ to 6 links, in a circular area of radius $r = 100$ meters, for path loss exponents in the interval [2, 5). For each test we would randomly place the N receivers and N transmitters and examine all $N!$ possible matchings. The reason we did not

examine matchings of more than six links was twofold: first this simulation required the time-consuming calculation of $6!\times10^5 = 72\times10^6$ eigenvalues of 6×6 matrices and second more important, the results obtained up to $N = 6$ (Fig. 2.2) were already conclusive.

In figure 2.2a, the $N = 2$, $\theta = 1$ line clearly complements the finding on the feasibility of matchings of Borbash and Ephremides in [B'04], according to which if $\theta = 1$ one at most matching will be feasible. The same can be readily observed in 2.2b for $N = 2$ for the line of $\theta = 1$: Since here we have two candidate links the feasibility probability will be 0.5. One more observation is suggested: as the exponent increases the probability for a matching to be feasible is reduced. In figure 2.2b we look at 20 curves each for a θ value from 0.05 down to 1 with a step of 0.05.

Through simulations we have verified another significant observation: *For a given* 2×2 *matching with* $\theta_1=\theta_2=\theta < 1$ *if feasibility is established at a path loss exponent value* n_f*, then feasibility is guaranteed for any exponent* $n < n_f$*.*

To prove this assume a 2×2 matching having $F = \theta \cdot \begin{bmatrix} 0 & \frac{G_{12}}{G_{11}} \\ \frac{G_{21}}{G_{22}} & 0 \end{bmatrix}$. The Perron eigenvalue of F is the positive solution of: $\rho_F{}^2 - \theta^2 \frac{G_{12}}{G_{11}} \frac{G_{21}}{G_{22}} = 0$, which taking eq.(1) into account becomes: $\rho_F = \theta \left(\frac{d_{12}}{d_{11}} \frac{d_{21}}{d_{22}} \right)^{-\frac{n}{2}}$. Since $f(x) = k^{-x}$ converges to 1 as x goes to 0, ρ_F similarly converges to θ, as n goes to 0. Given the monotonicity of $f(x) = k^{-x}$ and that for n_f we have $\rho_F < 1$, ρ_F will remain below 1 for all values of $n < n_f$.

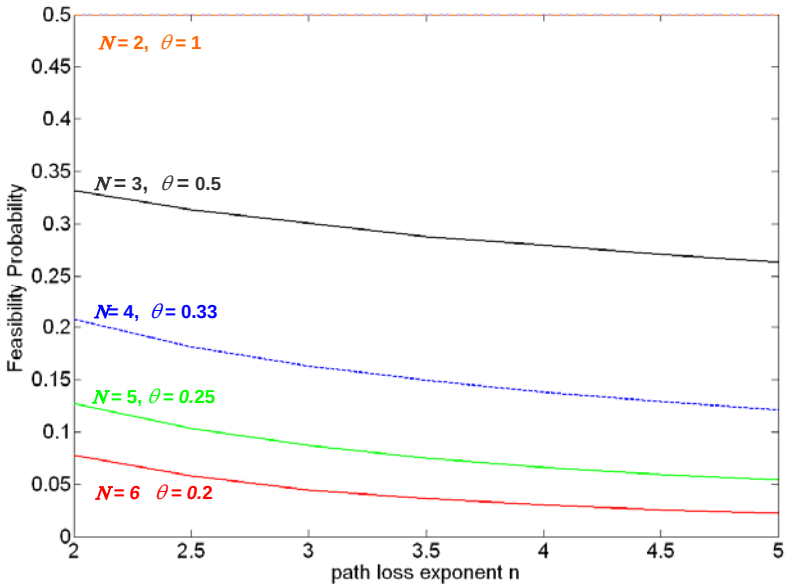

(a)

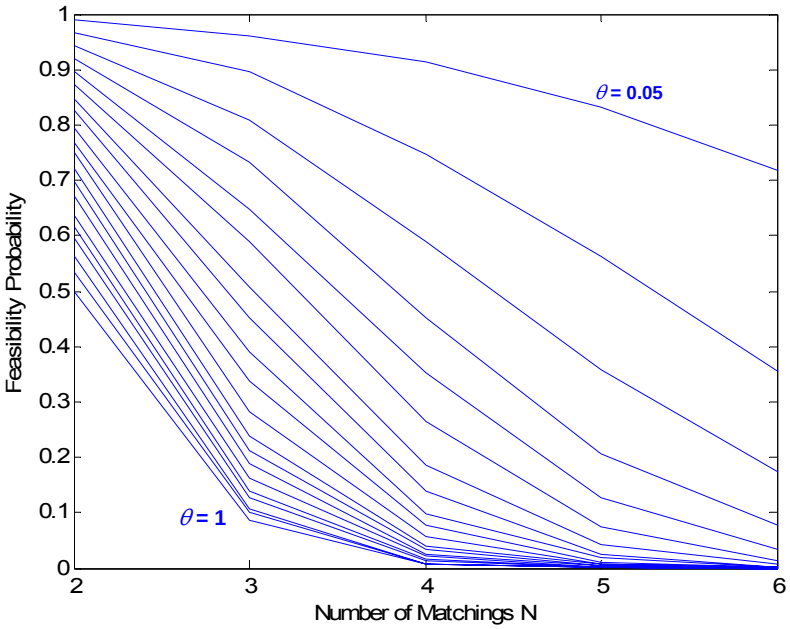

(b)

Figure 2.2: *Probability of a matching feasibility* (a) *vs. the path loss exponent n and(b) vs. the matching size for θ = 0.05 (top) down to θ =1 (bottom), for n =2.*

This can be seen as a simple lemma of a far more general conjecture supported by simulations (Fig. 2.3): *The Perron eigenvalue of a matrix in the form of F having* $\theta_i = \theta \; \forall \, i \in [1, N]$ *converges to* $\theta \cdot (N - 1)$ *when* $n \to 0$.

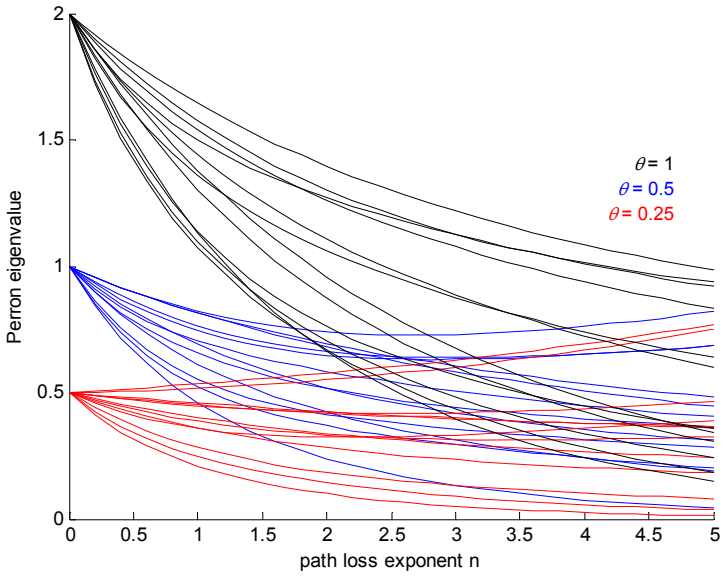

Figure 2.3: *The Perron eigenvalue converging to (N-1)θ as the exponent n decreases to 0. Illustrating a dozen random topologies of N = 3, with θ values of 1, 0.5, and 0.25*

Our next two findings focus on the mean transmitter and aggregate network power per time-slot. In figure 2.4, we see that the mean transmitter power is exponentially increasing with the path loss exponent *n*. We see that, regardless of the density of the network, for an increase of the path loss exponent by half a unit, the mean transmission power goes up by an order of magnitude. On the other hand increasing the number of links by one, the *per node* power cost increases by a small amount, which is independent of the path loss exponent. However, this observation has to be viewed in conjunction with the result in figure 2.2: The power cost to add one more link to the matching may be low, but the new resulting ***super-matching*** is less likely to be feasible.

From the simulations we have also seen that the assigned aggregate transmission power follows closely a gamma distribution, whose parameters depend on the path loss exponent *n* (Fig. 2.5). This observation could be linked to an analytical result by Haenggi in [H'05], according to which, the link lengths in a uniformly distributed ad hoc network follow the gamma distribution. In simulations we have also verified this analytical result.

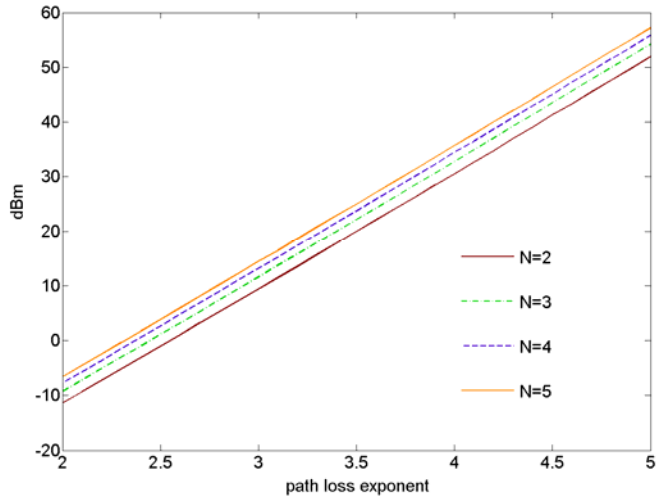

Figure 2.4: *Mean transmission node power in dBm, vs. the path loss exponent n, for varying matching sizes in a circular area of r = 100m*

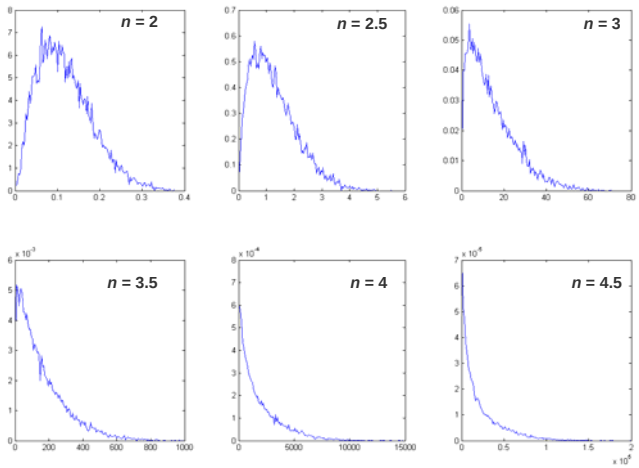

Figure 2.5: *Empirical probability density function of the aggregate transmitted power in mW, at a time-slot for a network of N=3 in a circular area of r = 100m.*

B. *On The Minimum Power & Maximum SINR Solutions*

In [GVGZ'93] Grandhi et. al. use the Perron eigenvalue ρ_A of the matrix:

$$A = \begin{cases} 0 & , i = j \\ \dfrac{G_{ij}}{G_{ii}} & , i \neq j \end{cases}$$

to calculate the maximum common SIR value $\theta_0 = \rho_A^{-1}$ which can be achieved by the given matching described by matrix A, in the absence of noise. This SIR is attained if the Perron eigenvector is used as a power vector. In [BE'04] Borbash & Ephremides showed that, when noise is present scaling the Perron eigenvector by an appropriate factor and using this as a power vector it is possible to get an SINR arbitrarily close to the maximum common θ_0 value. Such a power assignment though is not optimum, in a minimum per transmitter output power sense, as can be seen in the figure 2.6, where the grayed area is the power feasibility region (see fig.A.2), for the noisy case. Forming the appropriate $F = \theta_0$A matrix and solving eq.(2.4) the actual minimum power vector P^* is obtained which achieves the exact solution for all the nodes to have the SINR required with the minimum power allocation.

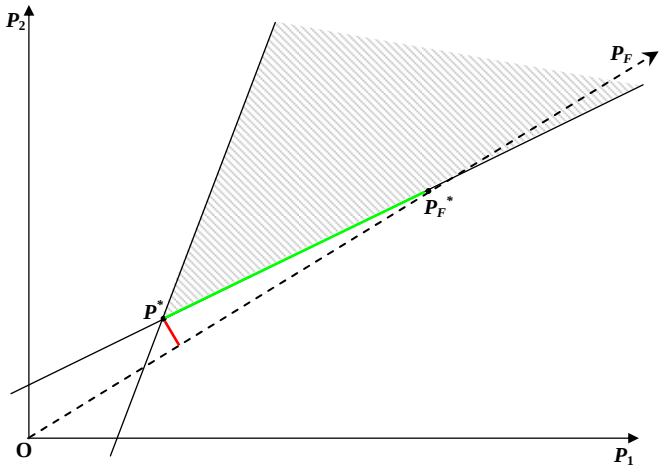

Figure 2.6: *Relation between the Perron eigenvector P_F and the minimum power vector P^* for a 2×2 matching, superimposed on the power feasibility region for the noisy case*

Also, in the course of our investigations for the relationship between mean transmission node power and the path loss exponent *n*, we observed and verified through extensive stimulations, that: *in irreducible matrices with elements of the form* $A_{ij} = [\ a_{ij}{}^{n}\ ]$, *with* $a_{ii} = 0$ *and* $a_{ij} > 0$, *for* $i \neq j$ *the sum of the components of the normalized Perron eigenvector of A decreases as n increases.*

This finding implies that in the case where the Perron eigenvector is used as a power assignment method then the distribution of transmission powers will be more skewed as the path loss exponent increases. The proof of this statement, in the $N = 2$ case, follows below:

Let us assume $A = \begin{bmatrix} 0 & a^x \\ b^x & 0 \end{bmatrix}$, $a > 0$, $b > 0$ and $x \in \mathbb{R}^+$.

Then its eigenvalues ρ_A are: $\det(A - \rho_A \mathrm{I}_2) = 0 \Leftrightarrow \det\begin{bmatrix} -\rho_A & a^x \\ b^x & -\rho_A \end{bmatrix} = 0$

$\Leftrightarrow \rho_A = \pm\sqrt{a^x b^x}$.

Hence the Perron eigenvalue of A is: $\rho_A^* = \sqrt{a^x b^x}$ and so the Perron eigenvector P_A^* can be found from:

$$\left(A - \rho_A^* \mathrm{I}_2\right) P_A^* = 0 \Leftrightarrow \begin{bmatrix} -\sqrt{a^x b^x} & a^x \\ b^x & -\sqrt{a^x b^x} \end{bmatrix} \begin{bmatrix} p_1 \\ p_2 \end{bmatrix} = 0$$

$$\Leftrightarrow \begin{vmatrix} -\sqrt{a^x b^x}\, p_1 + a^x p_2 = 0 \\ b^x p_1 - \sqrt{a^x b^x}\, p_2 = 0 \end{vmatrix} \Rightarrow P_A^* = p_1 \begin{bmatrix} 1 & \sqrt{\left(\frac{b}{a}\right)^x} \end{bmatrix}^T, p_1 \in \mathbb{R}^+,$$

since the Perron Eigenvector has all-positive elements.[2]

[2] p_1 could, out-of context, be chosen to be negative; in such a case the property we prove would be restated as: "*the sum S of the* ***absolute values*** *of the elements of the normalized Perron eigenvector of A is a decreasing function of the exponent x*". The proof is the same in both cases.

For the trivial case of $a = b$: $P_A^* = p_1 \begin{bmatrix} 1 \\ 1 \end{bmatrix}$, regardless of x. [3]

We shall now show that, in all other cases, the sum S of the elements of the normalized Perron eigenvector of A is a decreasing function of the exponent x:

The norm of the Perron eigenvector is then: $\left\| P_A^* \right\| = p_1 \sqrt{1 + \left(\frac{b}{a} \right)^x}$, so the sum of the elements of the normalized Perron eigenvector is:

$S(x) = \frac{1 + \sqrt{\left(\frac{b}{a} \right)^x}}{\sqrt{1 + \left(\frac{b}{a} \right)^x}}$. Taking $c = \frac{b}{a} \in \mathbb{R}^+ \setminus \{1\}$, we have $S(x) = \frac{1 + \sqrt{c^x}}{\sqrt{1 + c^x}}$.

We want to examine the monotonicity of S with respect to x, so:

$$\frac{dS}{dx} = \frac{d \frac{1 + \sqrt{c^x}}{\sqrt{1 + c^x}}}{dx} = \frac{\left(\sqrt{1 + c^x} \right) \cdot d\left(1 + \sqrt{c^x} \right) / dx - \left(1 + \sqrt{c^x} \right) \cdot d\left(\sqrt{1 + c^x} \right) / dx}{1 + c^x},$$

since $1+c^x > 0$ we just need to examine the sign of the numerator:

$$N = \left(\sqrt{1 + c^x} \right) \cdot d\left(1 + \sqrt{c^x} \right) / dx - \left(1 + \sqrt{c^x} \right) \cdot d\left(\sqrt{1 + c^x} \right) / dx = \frac{\sqrt{c^x} \ln c}{2} \left(\frac{\left(1 - \sqrt{c^x} \right)^2}{1 - c^x} \right).$$

In any case: $\left(1 - \sqrt{c^x} \right)^2 > 0$ and $\sqrt{c^x} > 0$

For $c < 1$: $\ln c < 0$, while $1 - c^x > 0$, for all $x > 0$; so $N < 0$

While for $c > 1$: $\ln c > 0$, while $1 - c^x < 0$, for all $x > 0$; so again $N < 0$

Since N is negative for any positive value of $c \neq 1$, then S is indeed a decreasing function of x.

[3] In the power control context this would map to the case of a completely symmetric topology of two links having equal link path losses G_{ii} and equal interference path losses G_{ij}. In this case it is intuitively obvious that the transmitters must have equal transmit powers to successfully operate their links

2.2 JAMMING NODES

This section provides a detailed study on a hypothetical application scenario, examining how jammers can affect the throughput and power assignment in an interference-limited network, under the model we have developed in the previous section.

The jammers we consider are devices able to transmit at the same frequency, occupying at least the same bandwidth, as the communication channel used by the network. They are assumed to be equipped with a single omnidirectional antenna and depending on the scenario may have different potential with respect to their computational, power adaptation and mobility capabilities.

We begin by making initially the assumption that the network will not be able to adapt its transmission powers. Should such a network operate under the optimum minimal power assignment of P^*, the slightest interference or noise power fluctuation would bring the entire network down. For this reason we further assume that the network initially has a provision of a reasonable safety margin of a several decibels above the θ_i thresholds in its SINR. This case is studied to derive basic relations concerning jammer location and transmission power requirements.

Following, we examine the case where the network can adapt its powers in a dynamically changing environment, under the constraint of a maximum power output for its transmitters. In this case the network can be considered to follow the Foscini-Miljanic algorithm and is also allowed to remove links from the matching when it becomes infeasible. This action is driven by the findings of the previous section: smaller matchings are more likely to be feasible. Also, intuitively, it results in reducing the interference

generated by the transmitter of the removed link and thus such an action can provide a reduced size feasible matching.

More specifically, in both the non-adaptive and the adaptive cases, our goal is to quantify the minimum energy required to bring out of operation a certain portion of the network. In the non-adaptive case we examine the following issues: first, the relation between jammer transmission power and link outage probability and second the per jammer power for scenarios of more than one jammers

Finally we examine the location of the jammer through simulations. We begin by generally examining networks where their perimeter is safe and examine by simulations the jammer advantage if placed inside the perimeter of the network, against scenarios where the jammer can only be placed on the perimeter, or further away from it.

In the adaptive case, we assume that the network will react to the jammers' effect as if the noise level had increased. If at some time-slot a receiver detects it has fallen below the required SINR threshold, the network will try to re-assign larger transmission powers to its transmitters to cope with the new environment conditions.

At this point a "turn-based game" begins, where in each round (time-slot) the jammer(s) increase their powers while the network compensates by increasing its transmitters' powers, until the power required by some transmitter will be above its maximum. Then, the network cannot compensate anymore by adjusting powers for the given matching; the only option for it is to remove one of its links. The selection is simple: remove the one having the maxed-out transmitter. This will result in reducing its interference and thus the remaining links will be able operate now at a lower power level. On the other hand, the jammers, at that point have the minimum power configuration

required to take out the first unit of throughput from the network. Falling below this configuration will enable the network to re-establish the broken link and so reducing the power is not an option for the jammers.

Through simulation we studied both these network cases (non-adaptive and adaptive). Our conclusion is that using two or more jammers, that cooperate to find their optimum transmission power, is comparable, in terms of total jamming power, to using a single jammer, but requires the coordination of the jammers in order to achieve it. We have also concluded that in the case of an adaptive network the aggregate jammer power is exponentially increasing with the number of links to be disabled. Even though the network is attempting to respond by increasing its power, the jammers do not have to use more power than in the case of a non-adaptive network, to bring the entire network down.

A. *JAMMER MODEL DESCRIPTION*

At a given time-slot t for a set of K jammers we want to find the non-negative power vector:

$$P_X = \left[p_{X^1}, p_{X^2}, ..., p_{X^K} \right]^T,$$

to minimize: $\sum_{i=1}^{K} P_{x_i}$,

achieving:
$$\frac{P_i G_{ii}}{\sum_{j \neq i} P_j G_{ij} + \nu_i + J_i} < \theta_i \qquad (2.6)$$

for each receiver i that we wish to bring below its SINR threshold.

In (6), J_i denotes the jammers' power on receiver i, and is given by:

$$J_i = \sum_{j=1}^{K} g_{ij} p_{X_i} = G_i^X \cdot P_X \qquad (2.7)$$

with g_{ij} denoting the path gain for jammer j to receiver i and $G_i^X = [g_{i1},...,g_{iK}]$ being the line-vector of all jammers' path gains to receiver i.

In order to find the minimum jammer power vector, we used the method of simulated annealing [KGV'83]. Our choice to use this heuristic algorithm proved sound, as the implementation and tuning of the annealing method was very fast to converge to robust estimations of minimum jammer power vectors. This process can be performed off-line for a non-adaptive case.

The simulated annealing algorithm is an iterative procedure: It begins with an estimation of the solution. At every iteration the algorithm takes a number of steps away from the estimated solution. At each step it examines a random neighbour of the previously estimated solution. If a neighbour is better in terms of the cost function, then it is kept as the current solution estimate and the algorithm proceeds to make a new step. If not, then the neighbour may still be accepted as an estimated solution, with a probability that depends on: (a) the iteration number and (b) a metric that quantifies the quality of the neighbour, compared to the estimated solution of the previous step. This is done in order to escape possible local minima. The iteration is complete either when a predefined number of "positive" estimates is made, or the number of "negative" accepted neighbours reaches a threshold. The algorithm concludes when either a predefined number of iterations is reached, or when no better neighbour can be found during an iteration.

In our case the solution is a jammer power vector P_X of minimum aggregate power, which lies in the region described by eq.(2.6). The "neighbour-space" contains the jammer power vectors that satisfy the constraint in eq. (2.6). A random neighbour of an estimated jammer power vector is a new vec-

tor in which only one element, picked at random, is slightly altered. Finally, the cost function is the aggregate jammer power we wish to minimize.

B. *RESULTS FROM SIMULATIONS*

Initially we tested how a single jammer can affect the network in the non-adaptive case. Our first target was to characterize the power requirements to progressively take out the links in the network (Fig. 2.7). The parameters that affect this are the path loss exponent, the network density, and the jammer location.

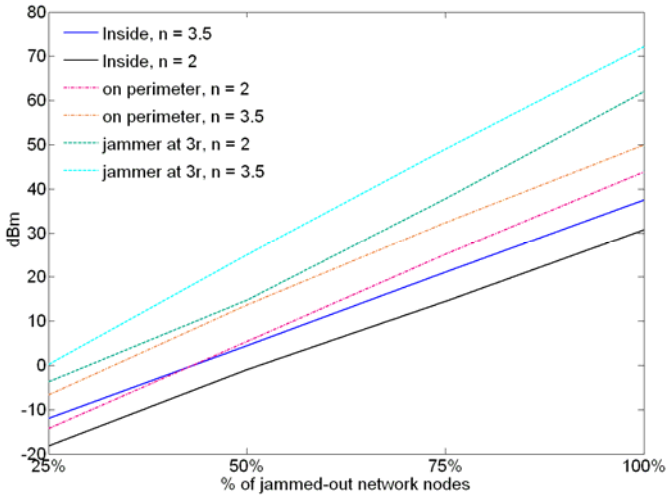

Figure 2.7: *Jammer power, for single jammer inside, on and away from the perimeter of the network, for path loss exponents of n=2 and n=3.5, N = 4, for a circular area of R =100m.*

In order for all the receivers of the network to receive their respective transmissions below the SINR threshold a given amount of interference power has to reach each receiver. This interference power can be generated by a single jammer, or multiple, cooperating, jammers in the network. In Figure 2.8 we see that this interference power requirement corresponds to the power aggregately transmitted by the jammers. For example in the case of n = 3.5 a sin-

gle jammer, is required to transmit at a power of 30dBm. At the same setup the 2 jammers annealing solution, (optimum solution), yields that the expected minimum value for each is 27dBm, over a large number of random jammer locations, for a total of 30dBm. Therefore using more jammers may result in each one producing less transmit power, but the total transmitted power by this coalition of randomly placed jammers is comparable to the power required by a single jammer. Although using more jammers may result in battery saving on each node, thus jamming for a longer duration, it requires the jammers to be able to exchange the information of the annealing solution to actually produce their minimum power vector.

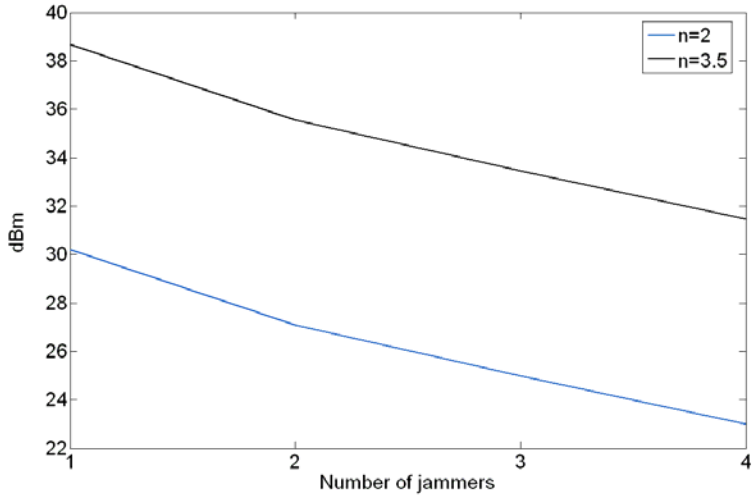

Figure 2.8: *Mean power per jammer to bring out all network links. N = 4*

We show a typical result for the adaptive case in figure 2.9. As we see, even though the network is increasing its power to adapt to a more "noisy" environment, this affects the jammers only while they take out the most vulnerable to them link. In the end, the jammers do not need to use more aggregate power than what is required in the non-adaptive case, to bring the entire net-

work down. This indicates that a network attempting to counter the jammers' effect simply produces too much interference to itself.

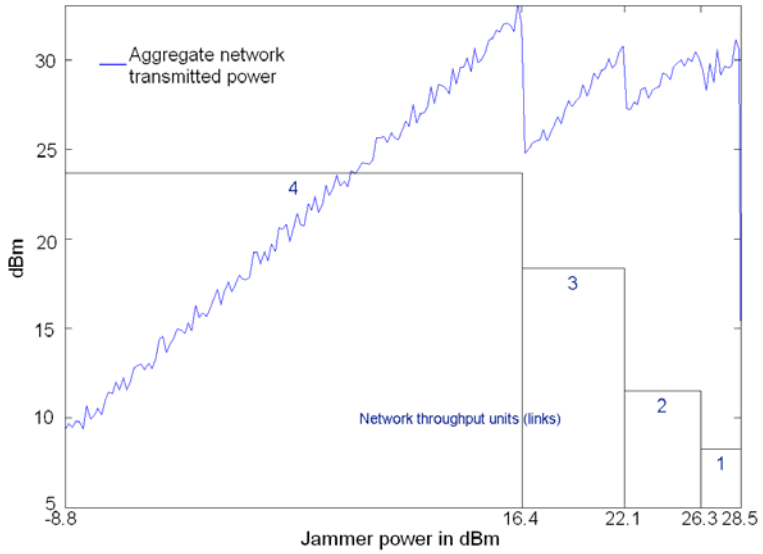

Figure 2.9: *The aggregate transmit power in an adaptive network of initially N=4 links vs. the power used by a jammer to take out the network links one-by-one.*

C. *Optimizing A Mobile Jammer*

Having these results at hand, we further investigated into how a single jammer could even more efficiently harm such a network. To this end we present a scenario which includes a jammer, with advanced computing, sensing, and mobility capabilities. We illustrate how such a node following a procedure using probing transmissions procedure, combined with the simplest possible movements pattern, will be able to discover the topology of a network, assuming that the path loss follows eq.(2.1) with n = 2, i.e. the free space path loss model. Once the network topology is discovered the jammer can move to a position inside of the network perimeter that we show to be the one where it will need the least power to bring the entire network down.

We describe the procedure for the tractable case of a 2×2 adaptive network below:

PHASE 1: Discovering the network topology

-STEP 1: *Finding the transmitters*

We assume the jammer is placed in a random position, which we will consider as the origin O = (0, 0) of a Cartesian set of coordinates.

Initially the jammer can detect the two signals from the two transmitters Tx_1 and Tx_2. We denote as *rss* (·) the received power from a transmitter and so:

$$A = rss(Tx_1) = P_1 \cdot G_{J1} = P_1 L \cdot d_{J1}^{-2} \tag{2.8}$$

$$B = rss(Tx_2) = P_2 \cdot G_{J2} = P_2 L \cdot d_{J2}^{-2} \tag{2.9}$$

Where $[P_1, P_2]^T = P^*$ is the power vector of the transmitters in the network.

If P^* was known, then equations (2.8) and (2.9) would suffice to provide d_{J2}, d_{J2}. Otherwise we move the jammer to a known position (x' , 0) and get the new values of *rss*.

$$A' = rss'(Tx_1) = P_1 \cdot G'_{J1} = P_1 L \cdot d'^{-2}_{J1} \tag{2.10}$$

$$B' = rss'(Tx_2) = P_2 \cdot G'_{J2} = P_2 L \cdot d'^{-2}_{J2} \tag{2.11}$$

Assuming Tx_1 lies in (x_1 , y_1) and Tx_2 in (x_2 , y_2) taking: A/A' and B/B' we obtain:

$$A / A' = P_1 L \cdot d_{J1}^{-2} / P_1 L \cdot d'^{-2}_{J1} = d'^{2}_{J1} / d_{J1}^{2} = \frac{(x_1 + x')^2 + y_1^2}{x_1^2 + y_1^2} \tag{2.12}$$

$$B / B' = P_2 L \cdot d_{J2}^{-2} / P_2 L \cdot d'^{-2}_{J2} = d'^{2}_{J2} / d_{J2}^{2} = \frac{(x_2 + x')^2 + y_2^2}{x_2^2 + y_2^2} \tag{2.13}$$

We need to make one more relocation of the jammer to (x'', 0) and similarly obtain a pair of new *rss* values A'' and B'', with which as in eq.(2.12) and (2.13) we obtain:

$$A/A'' = P_1 L \cdot d_{J1}^{-2} / P_1 L \cdot d'^{-2}_{J1} = d'^{2}_{J1} / d_{J1}^{2} = \frac{(x_1 + x'')^2 + y_1^2}{x_1^2 + y_1^2} \tag{2.14}$$

$$B/B'' = P_2 L \cdot d_{J2}^{-2} / P_2 L \cdot d'^{-2}_{J2} = d'^{2}_{J2} / d_{J2}^{2} = \frac{(x_2 + x'')^2 + y_2^2}{x_2^2 + y_2^2} \tag{2.15}$$

So, having the four equations (2.12) though (2.15) we can solve for $|x_1|$, $|y_1|$, $|x_2|$, $|y_2|$. Two more such measurements are needed in order to recover the signs from the absolute values and so the positions of the transmitters can be discovered.

-STEP 2: *Finding the receivers*

At the previous step the jammer performed passive measurements and repositioned itself in order to obtain the locations of the transmitters. In order to locate the receivers, the jammer must fire up its transmitter and observe the way with which the network alters its power vector. The key here is the observation that, if the jammer affects the SINR threshold so that the network tries to maintain at a certain value, then the network will use a new power vector so that the resulting new SINR is again equal to the threshold.

Assume that the initial unknown to the jammer SINRs are:

$$SINR_1 = \frac{P_1 G_{11}}{\nu + P_2 G_{12}} \tag{2.16}$$

$$SINR_2 = \frac{P_2 G_{22}}{\nu + P_1 G_{21}} \tag{2.17}$$

With $[P_1, P_2]^T = P^*$ the initial power vector.

Since in step 1 above the jammer located the transmitters, equations (2.10) and (2.11) can be used again to calculate P^*. Still in eq.(2.16) and (2.17) all four loss factors and both the *SINR* thresholds are unknown.

Now, let the jammer start transmitting with P_J sufficiently large. The network will attempt to compensate and reset its powers to a new vector $[P_1', P_2']^T = P^{*}'$ such that:

$$SINR_1 = \frac{P_1' G_{11}}{\nu + P_2' G_{12} + P_J G_{1J}} \tag{2.18}$$

$$SINR_2 = \frac{P_2' G_{22}}{\nu + P_1' G_{21} + P_J G_{2J}} \tag{2.19}$$

Again the new vector P^{*}' can be recovered by the jammer using equations (2.10) & (2.11). Equations (2.18) and (2.19) contain now the loss factors of the paths from the jammer to the receivers, which are two more unknowns and so equations (2.16) through (2.19) have a total of 8 unknowns. Still, one can observe that any P_J alteration will result a new pair of equations with the same unknowns as eq.(2.18) and eq.(2.19) , hence with two such more jammer power alterations four more independent equations can be generated and all loss factors can be discivered.

Once all loss factors are discovered, the distances between transmitters and receivers, as well as the distances of the jammer from the receivers, can be calculated using eq.(2.1). As we saw in step 1 this will result in discovering two potential locations for each receiver. In order to obtain the real position the jammer has to move and perform the same probing procedure again, as illustrated in figure 2.10 for one of the two receivers in the 2×2 matching.

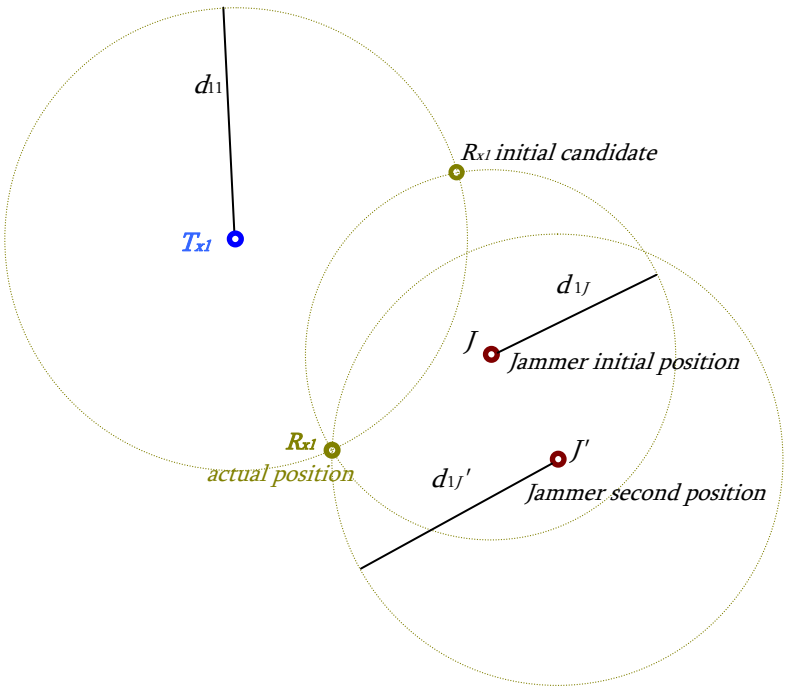

Figure 2.10: *Receiver positions discovery by a jammer.*

PHASE 2: Optimal Jamming Positioning

Having concluded phase 1, the jammer is fully aware of the network topology. In this phase we aim to find and move the jammer to the position that best utilizes its transmitted power. Our criterion for optimality in jammer power utilization is to minimize the aggregate SINR in the network.

First of all we shall begin by showing that the optimum position for the jammer lies on the line segment connecting the two receivers. Let us consider placing a jammer, transmitting at a given power, on any point say X on the line ε which connects the two receivers. Consider the perpendicular ε' of ε passing through X. Moving the jammer on any point X' on ε' results in increasing its distance from both receivers, hence due to eq.(2.1) the influence of the jammer in both receivers is less than what it would have been on X. Since any point on the plane can be considered to lie on a line perpendicular to ε there cannot be a point outside of those on ε that has more impact on the ag-

gregate SINR. With similar arguments the optimum point is confined within the line segment connecting the two receivers.

Having confined the problem for optimal position in a 1-d space, we assume line ε to be the x-axis, receiver Rx_1 to be on the origin $x=0$ and that Rx_2 lies on $x=D$ (known to jammer). Then the optimal solution is obtained by solving:

$$\arg\min_x(SINR_1 + SINR_2) = \arg\min_x\left(\frac{P_1G_{11}}{\nu + P_2G_{12} + P_JG_{1J}} + \frac{P_2G_{22}}{\nu + P_1G_{21} + P_JG_{2J}}\right) \quad (2.20)$$

where all but G_{1J}, G_{2J} are independent of the position of the jammer, while from eq(2.1): $G_{1J} = L \cdot x^{-2}$ and $G_{2J} = L \cdot (D-x)^{-2}$. Replacing in these in eq(2.20) above, and taking the derivative on x we have to solve a a 5th order polynomial which in [0,D] is convex and has a single minimum.

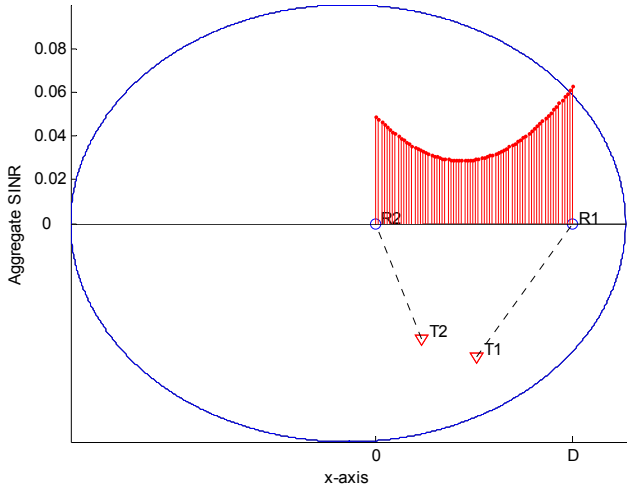

Figure 2.11: *The aggregate SINR in a network of 2 links for a jammer moving on the line segment connecting the receivers superimposed on a 2×2 network.*

Phase 3: Jammer power game

Once located in the optimal position the jammer has only to start powering up and detecting the network behavior, following the strategy presented

in the previous phases. Simply increasing its transmission power whenever the network transmitters increase theirs from this position will bring the entire network down with minimum power spending.

2.3 CONCLUSION

In this chapter we presented a thorough study of well-known power assignment methods in a wireless ad hoc network. We examined how typical low-layer wireless network parameters such as network density and environment variables, such as the path loss exponent, can affect the power assignment to the transmitters and the feasibility of random matchings.

We provided insights for the feasibility probability of a matching with respect to its size, its SINR threshold and the path loss environment. We also provided structural findings on the properties of the Perron eigenvalue and the sum of the elements of the normalized Perron eigenvector of matrices of the form used in the power assignment solutions for the noiseless and noisy case.

Furthermore, we examined how malicious jamming nodes can reduce the aggregate capacity of an interference-limited network, breaking its connectivity and whether an adaptive network can mitigate these jamming attempts, by simply adapting its transmitting powers. For the latter the answer was negative. We also established that using more than one jamming nodes does not require to spend more power on average, at the cost of having more complex jamming nodes that need to cooperate in order to be able to use the minimum jamming power. Finally we proposed a strategy, to minimize the power cost, for a single mobile jammer with increased computational capability in order to harm an adaptive network.

3
PORTING THE SINR CRITERION IN A MULTI-CHANNEL SYSTEM

As we saw in the previous chapter the SINR criterion for the successful capture of the transmitted data at a receiver, requires that the Signal to Interference-plus-Noise ratio must be at least equal to a threshold θ which depends on the transmission rate, the modulation scheme, and the required bit-error-rate. In a simple ad hoc single-interface, single-channel system, as the one examined in the previous chapter, eq.(2.2) is the mathematical model for the SINR criterion.

In this chapter we examine how this model can be extended to cover more complex networks that may have nodes with more radio-interfaces, use directional antennas and operate on more than one channel. We present an enhanced model that takes Adjacent Channel Interference (ACI) into account for the SINR calculation and apply it in the popular IEEE 802.11a/b/g suite of standards. Our model successfully quantifies the ACI generated by partially overlapping neighboring channels. We apply the model on a laboratory testbed and examine how it can be used to predict throughput in a controlled environment, and finally we evaluate its accuracy on an outdoors testbed, where we integrate it in a link budget calculation that also takes into account the antennas employed by the nodes.

3.1 QUANTIFYING ACI

In the previous chapter in eq.(2.2) interference at a receiver was calculated as the sum of the received power transmitted by neighboring same-channel transmitters. If we assume that our system uses not only a single channel but also neighboring channels that partially overlap, then this overlap has to be taken into account on the ACI calculation. We therefore generalize eq.(2.2), introducing a factor ξ that primarily quantifies this overlap and so the interference at a receiver i is calculated as:

$$I_i = \sum_{j \neq i} P_j \cdot \xi_{j,i} \cdot G_{j,i} \tag{3.1}$$

where P_j is the transmitting power of node j, $G_{j,i}$ is the interference path loss from transmitter j to receiver i and the factor $\xi_{j,i}$ depends on the spectral properties of the channels and signals used, and the separation between the channels of the interferer j and the receiver i. Specifically, the effective properties are the inter-channel spectral distance, the channel bandwidth, the spectral mask[4] and the receiver filter. As it is obvious, if links i and j use the same channel then $\xi_{j,i} = 1$, and so we eq.(3.1) is reduced to eq.(2.2).

We calculate the ξ factor by normalizing the spectral mask $S(f)$ within a bound w that will be at least equal to the nominal channel width and then filter this normalized $S'(f)$ over the frequencies that will be within the band-bass filter of the receiver. Ideally this should be a flat band-pass 20MHz filter, but typically the assumption of a single imperfect, wider than nominal, band-pass filter used for transmission and reception is valid, and so in the general case we have:

[4] The **transmit spectral mask** is the power contained in a specified frequency bandwidth at certain offsets, relative to the total carrier power.

$$S'(f) = \frac{S(f)}{\int_{\frac{-w}{2}}^{\frac{w}{2}} S(f)df} \tag{3.2}$$

Where w is the receiver filter bandwidth. Denoting the receiver filter transfer function as $R(f)$ we similarly normalize it to $R'(f)$ within $[-w/2, w/2]$ we have:

$$\xi_{i,j} = \int_{\frac{-w}{2}}^{\frac{w}{2}} R'(f)S'(f)df \tag{3.3}$$

In a system where all radio interfaces adhere to the same protocol it is reasonable to assume that all nodes have the same $S(f)$ and furthermore that this "output filter" matches the receiver filter, that and so: $S(f) = R(f)$. Under these two assumptions eq.(3.3) becomes:

$$\xi_{i,j} = \int_{\frac{-w}{2}}^{\frac{w}{2}} S'(f)S'(f - f_{\text{int}})df \tag{3.4}$$

where we have denoted by f_{int} the frequency offset at which the interfering channel is centered (See fig 3.1)

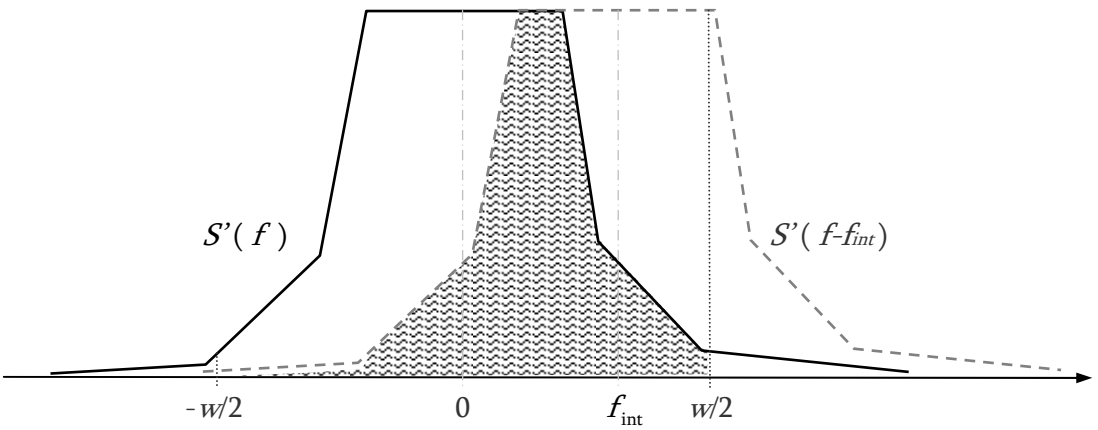

Figure 3.1: *Graphical representation of the calculation of eq.(3.4).*

Using our model and the spectral mask for the 802.11a mandated by the standard in [80211a'99] we analytically calculated the theoretical power leakage between two neighboring 802.11a channels. Table 3.1 shows the results of our calculations of the ACI ξ_{ij} factor expressed in dB.

TABLE 3.1
THEORETICALLY CALCULATED ξ_{ij} IN dB

Receiver Bandwidth	**Immediately Adjacent Channel** Power Leakage $\xi_{i(i+1)}$	**Next Adjacent Channel** Power Leakage $\xi_{i(i+2)}$
20Mhz	-22.04	-39.67
∞	-19.05	-36.67

These results indicate that: The interference factor is well above the thermal noise in an 802.11a system even when two channels separated by an unused channel are used (**next adjacent channel** column). Therefore ACI indeed exists in 802.11a, because of poor channel design, and if not properly handled can cause degradation to a system's performance. In order to demonstrate this and thus experimentally verify our model we constructed a testbed with off-the-shelf equipment.

Initially we chose to emulate the wireless medium, rather than using the real medium, in order to remove the non-deterministic characteristics of fast fading and shadowing, and so eliminate the inherent wireless medium uncertainty from our investigations. This led us to a laboratory testbed where nodes' RF connectors were interconnected using cables, attenuators, signal splitters and combiners. Our next step was to use the same node hardware to perform outdoors experiments using directional antennas, thus extending our work and the work in the literature to conduct an "**interference budget**" that takes into account not only the ACI factor, but also the radiation patterns of

the antennas used. Conducting an accurate interference budget is indeed important in the design of multi-radio multi-channel systems, because it can be the basis for a tool to design such systems installations. The next paragraph describes the two mechanisms that affect 802.11a throughput and gives the first insights on the experiments conducted to emulate them.

3.2 THE MECHANSISMS THAT ARE AFFECTED BY INTERFERENCE IN THE IEEE 802.11

A. *CLEAR CHANNEL ASSESSMENT FALSE NEGATIVES*

The IEEE 802.11a employs a carrier sense multiple access with collision avoidance (CSMA/CA) MAC protocol with binary exponential back-off, called distributed coordination function (DCF) The DCF defines a basic access mechanism and an optional request-to-send/clear-to-send (RTS/CTS) mechanism. We only consider the basic access mechanism, shown in figure 3.2.

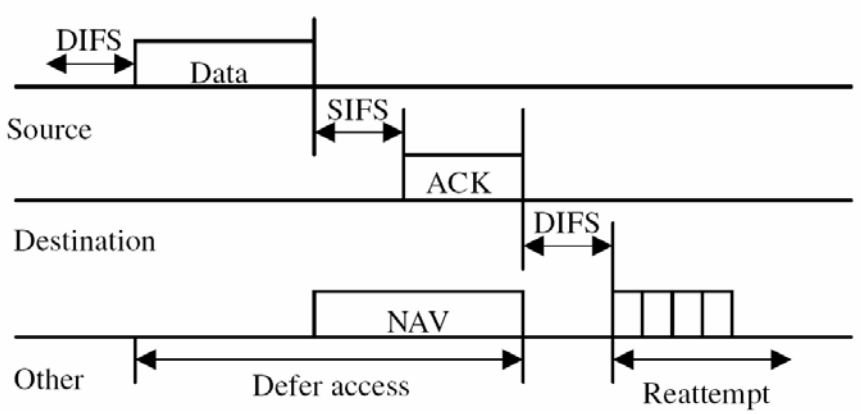

Figure 3.2: *The basic 802.11a Distributed Coordination Function (DCF).*

In the DCF a station has to sense the channel as clear (idle) for at least a duration of DIFS+CWmin (both defined in [802.11a'99]) in order to gain access to

it. The 802.11a standard requires that a Clear Channel Assessment (CCA) mechanism be provided by the physical layer. The CCA mechanism, that will provide this information, is to proclaim a channel as busy if it decodes a PHY layer preamble at a power at least equal to that of the basic rate of the 6Mbps sensitivity[5], or it detects any signal with power 20dB above the 6Mbps sensitivity. Table 3.2 below lists the sensitivity per rate required by the standard and those reported as typical by Cisco for its Aironet802.11a/b/g CardBus Adapter and by Ubiquiti for its SRC 802.11a/b/g Hi-Power Cardbus Adapter. For the CCA mechanism we must look at the first line of this table: the sensitivity for the basic 6Mbps rate.

TABLE 3.2
SENSITIVITY FOR THE TRANSMISSION RATES OF 802.11a

Transmission Rate (Mbps)	IEEE 802.11a	Cisco Aironet	Ubiquiti SRC
6	**-82**	**-87**	**-93**
9	-81	-87	-92
12	-79	-87	-90
18	-77	-87	-89
24	-74	-82	-87
36	-70	-79	-84
48	-66	-74	-78
54	-65	-72	-75

Interference can cause the CCA to misreport in the case of nearby located interfaces: A channel may be sensed as busy, due to high received power from a neighboring channel that is interfering. This can be considered as the case of two nearby 802.11a transmitters, that may contend over different channels. This is a case which can happen on a poorly deployed multi-radio node. For example one

[5] **Sensitivity** is the minimum input power level at which decoding can be achieved at a desired BER, in a given rate,.

that has two, or more interfaces using nearby channels, with omni- or directional antennas, with insufficient physical separation, or radio isolation between them.

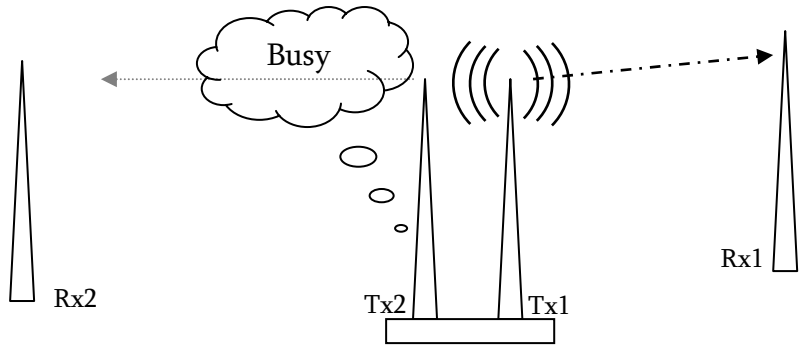

Figure 3.3: *Tx2 may report falsely the channel as busy if the* Tx2→Rx2 *channel is adjacent to the channel* Tx1→Rx1.

Example 3.1:

Consider that in the setup of figure 3.3 all nodes are equipped with typical indoor for the lower/middle U-NII 5GHz band, 5dBi omni-directional antennas. Tx1 is transmitting to Rx1 with 1mW on channel 56, while the link Tx2→Rx2 is set on the immediately adjacent channel 60. The interference budget calculated in dBs is:

$$B_{1\to 2} = Tx1\,Power + \xi_{1,2} + GantTx + GantRx + PathLoss(\text{Tx1}\to\text{Tx2}) \quad (3.5)$$

In order for the CCA not to have any false positives it would require that:

$$B < Sensitivity(6Mbps)+20\text{dB} \quad (3.6)$$

From eq.(3.6), if we consider a Cisco card as in table 3.2, with hard 20Mhz channel boundaries for table 3.1, we have:

$$PathLoss(\text{Tx1}\to\text{Tx2}) < -54.96 \quad (3.7)$$

Using a more specific free-space path loss model [R'02] than the one in the previous chapter, namely considering:

$$PathLoss(d)_{dB} = -(20log_{10}(d) + 20log_{10}(f_c) - 147.56) \quad (3.8)$$

where d is the path distance in meters, and f_c is the channel frequency, while the factor -147.56 accounts for the spherical propagation of the energy, we find that

the minimum distance between the two omni-directional antennas has to be at least 2.53m, assuming they are at the same elevation. Changing the transmission power to 50mW would result in a minimum distance of 17.9m. Placing the antennas closer together would result in the two transmitting stations to contend for the channel capture, even though they are operating on different channels. Equation 3.5 is the basic interference budget tool we propose for a multi-channel system. In the following we will introduce a more complete interference budgeting formula that also takes into account the use of directional antennas.

B. *DATA RECEPTION MECHANISM ERRORS*

The SINR Criterion we developed in Chapter 2 applies in the reception mechanism of 802.11a and directly affects the resulting effective throughput of a link as in [LYCZ'06]. Assuming that interference by other 802.11a stations (see Fig. 3.4) can be modeled as noise, given the SNR requirements for the 802.11a standard transmission rates we should be able to at least predict for given interference the rate at which a link will operate at the 10% Packet Error Rate (PER) for packets of 1000 bytes.

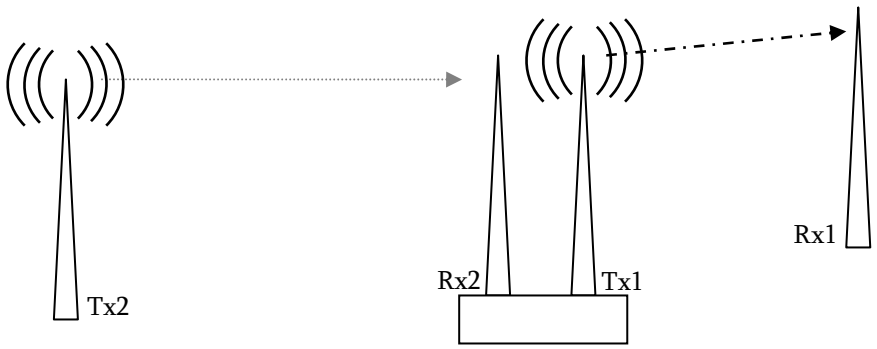

Figure 3.4: *Rx2 will not be able to correctly decode the data transmitted by* Tx2 *due to high interference from nearby channel transmission of Tx1.*

3.3 TESTBED SETUPS & EXPERIMENTS

A. *LABORATORY TESTBED MODEL VERIFICATION*

We conducted our experiments on a laboratory testbed platform of 4 laptops running the Ubuntu linux distribution based on the 2.6.20-16 kernel. The wireless interfaces we used were 4 Atheros-based Ubiquiti SRC a/b/g pcmcia cards running on the MadWifi-ng driver (svn 2594). We initially chose to emulate the wireless medium, removing the non-deterministic characteristics of fast fading and shadowing, in order to eliminate its uncertainty factors from our investigations. Therefore, we used signal splitters/combiners with a variety of fixed signal attenuators ranging from 3 to 50dB. We also used a Rohde&Schwarz FSH6 Spectrum Analyzer in order to verify the power levels at various points on the testbed, and the spectral masks produced by the wireless interfaces and thus validate our results in table 3.1. For UDP traffic generation we used the Iperf program (v2.0.2). Finally, we used the Airmagnet Laptop Analyzer (v.4), to have a sniffer's view of the actual 802.11a MAC layer. The testbed components are summarized in table 3.3 and Figure 3.5 displays the testbed in action.

Figure 3.5: *The indoors testbed.*

TABLE 3.3
TESTBED EQUIPMENT

A. Node Components

4x Laptops running on Ubuntu Linux 2.6.20-16
4x Atheros-based Ubiquiti SRC a/b/g pcmcia cards [U'08]
MadWifi-ng driver (svn 2594) [M'08] modified to:
- Disable Diversity
- Force Basic Rate at 6Mbps

Iperf traffic generation program (v2.0.2).

B. Link Components

i. Indoors
2 & 4 way Signal Splitters/Combiners
0-6GHz Signal Terminators
Signal Attenuators
fixed values: 50 dB (1x),
20, 10, 6, 3dB (2x).

ii. Outdoors
4x 19 dBi patch panel Interline antennas
4x 27 dBi patch panel Vesuvius Stream-line's antennas
[I'08,VS'08]

Variety of interconnecting 50Ω low-loss Coaxial Cables, Pigtails and Adapters.

C. Monitoring Tools

Rohde&Schwarz FSH6 Spectrum Analyzer [RS'08]
Airmagnet Laptop Analyzer (v.4) [AM'08]

1. *CCA TESTING*

With the setup of figure 3.6. we emulate the case of a baseline link ($T_1 \rightarrow R_1$) operating at channel 60, while a second transmitter T_2 is continuously pushing packets in an adjacent channel link, which is unable to sense the first. A key of our hardware infrastructure that enabled this design was the fact that the Ubiquiti SRC 802.11a/b/g radio interfaces we used were equipped with two antenna jacks. For this setup we were able to make the MadWifi driver successfully disable the antenna diversity feature at the Atheros chipset binary Hardware Abstraction Layer (HAL).

In the resulting setup of figure 3.6 based on the topology of figure 3.3, the roles of the two links are not quite symmetric: we have a **test link** with a

clear communication role $T_1 \rightarrow R_1$ and an **interfering link:** $T_2 \rightarrow R_2$. The test link is the one we will operate alone and record its performance in various settings of transmit rate and data throughput to establish the **baseline performance** and then compare it when the interfering link is operating with various parameters.

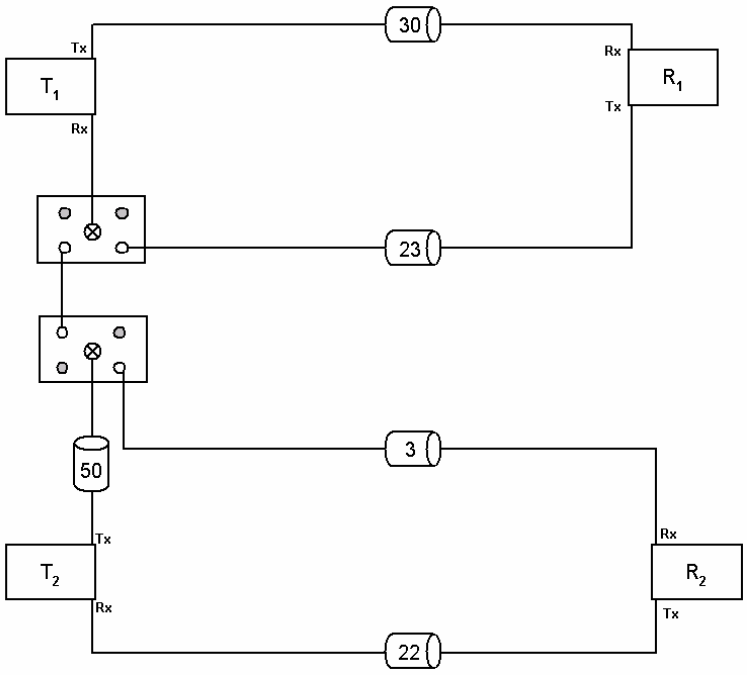

Figure 3.6: *Schematic of the testbed setup used the ACI effects on the CCA mechanism.*

One important detail is that although T_2 by construction constantly senses its channel as clear, it still has to comply to the MAC timings of 802.11a (fig 3.2), and so there are inter-packet periods at which the link ($T_2 \rightarrow R_2$) is idle. The values of the attenuators in figure 3.6 were so selected as to allow T_2 when set to a transmission power of 0dBm and tuned to channel 56 to affect the CCA mechanism of T_1. Channel 56 is according to 802.11a the immediately adjacent channel to channel 60. This interference budget is not sufficient to interfere with T_1, when T_2 is tuned to channel 52 (the next adjacent channel, two channels away from 60). Raising the power though to 18dBm results in

the overall power received by T_1 to just exceed the CCA threshold (which in our testbed case is the receiver sensitivity for the 6Mbps rate) and thus channel 60 will be falsely perceived as busy.

With this setup and with the help of the spectrum analyzer we were able to verify that the model we presented earlier for the calculation of the ACI factor ξ correctly predicts the leaked ACI power as the measured powers corresponded to the values of table 3.1. We therefore conducted experiments to measure the throughput of link $T_1 \rightarrow R_1$ under a high utilization in link $T_2 \rightarrow R_2$. For each 802.11a transmission rate, node T_1 would try to capture channel 60 in order to transmit UDP traffic of packets carrying 500, 1000 and 1500 bytes of payload, with a data rate as high as the transmission rate. In all the rest this was happening while at the same time link $T_2 \rightarrow R_2$ was already active in channel 56 producing immediately adjacent channel ACI, or in channel 52 producing next channel ACI, with a UDP transmission of packets of 1470 bytes payload, at the rate of 6Mbps, which yields a channel utilization of approximately 90%. An initial baseline scenario was recorded with only the $T_1 \rightarrow R_1$ test link active. Results presented in figure 3.7, for packets with 1000 bytes, indicate that the effect of ACI on the CCA mechanism is nearly binary in nature: if the received power in the sensing channel is high enough, regardless of the channel distance or the transmission power of the interfering transmitter, then the channel will be sensed as busy.

Still as one can observe, the affected channel is not rendered completely useless, some data does go through. As mentioned earlier the interferer used for this experiment was an 802.11a interface that obeyed the 802.11a DCF. That is, T_2 before each transmission would have to remain idle for a total of: SIFS and the time required to receive the acknowledgement of the previous transmission, plus another DIFS to sense the channel and then, since by con-

struction there is no contention in the $T_2 \rightarrow R_2$ link, another CWmin. This is the reason why the generated traffic would yield a channel utilization of 90%. In some cases this appears to be a period long enough for T_1 to successfully capture the channel and so push some data through to R_1.

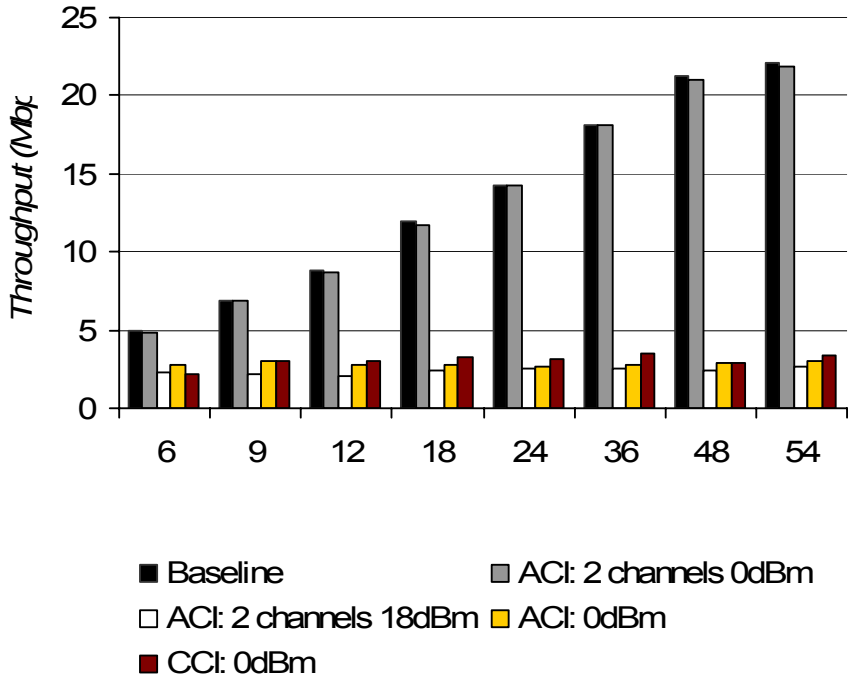

Figure 3.7: *The effect of ACI on throughput is nearly binary.*

2. INDOORS SINR TESTING

In order to examine the ACI effect on the 802.11a packet reception mechanism we set up the testbed as shown in figure 3.8. Here, the design became highly complicated because the MadWifi driver has still limited control on the binary Atheros HAL. Although we had disabled the antenna diversity feature and attempted to conduct our tests on a simpler testbed design than the one of fig.3.8 we observed that the antenna connectors would flip roles once the SINR was high enough to cause errors. Therefore we were forced to go to the testbed connection design in Fig. 3.8, where diversity is assumed not to be an option in link

$T_1 \rightarrow R_1$, and the attenuators are so chosen as not to invoke the CCA effect described earlier.

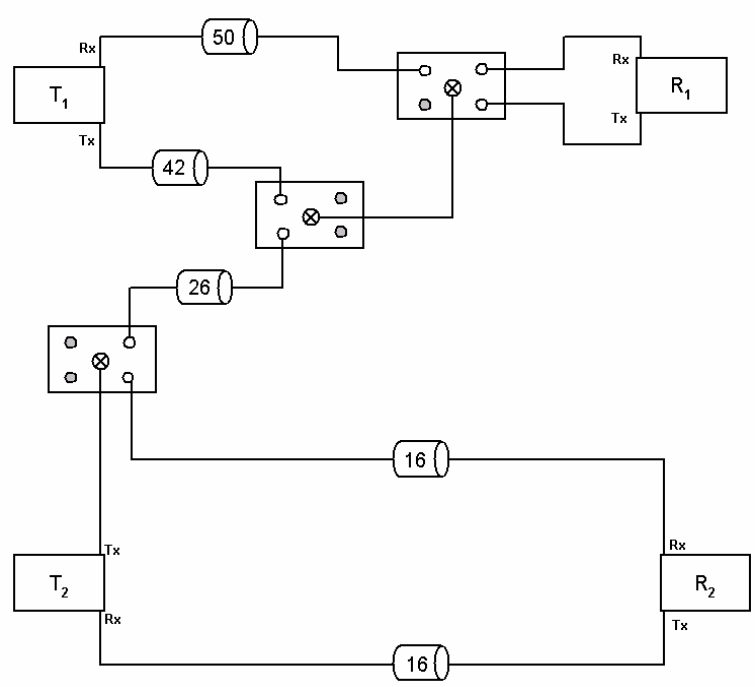

Figure 3.8: *Schematic of the testbed setup used the ACI effects on the data reception.*

From the receiver sensitivity of the SRC cards used we calculate the minimum SNR that is required for the card to receive at a transmit rate R:

$$ReceiverSensitivity(R) = SNRmin(R) + (N_f + N_{thermal}) \quad (3.9)$$

calculating $N_{thermal}$ using Boltzmann's equation[6] and assuming a noise-floor N_f of 2dB we produce the minimum SNR required for each rate, as in Table 3.3[7]. The SINR at the R1 in each transmission rate of T1 and each transmission power for T2 should be above the corresponding SNRmin, in order to achieve the theoreti-

[6] $N_{thermal} = K \cdot T \cdot B$, where Boltzmann's Constant $K = 1.38 \times 10^{-23}$ Joules/Kelvin, T is the environment temperature in Kelvin, and B is the Bandwidth in Hz.

[7] Although these SNR values can easily be analytically produced for the required Packet Error Rate of 802.11a of 10^{-1} for packets of 1000bytes, since the vendors try to differentiate their products those values will not be no more valid than the ones we produce in table 3.3.

cal BER mandated by the protocol and therefore the throughput of the baseline experiment (three first columns in table 3.4).

TABLE 3.3
CALCULATED SNRmin IN dB

Tx Rate	6	9	12	18	24	36	48	54
SNRmin	4.8	5.8	7.8	8.8	12.8	15.8	21.8	24.8

In the experiment we present in Fig. 3.9, with results in table 3.4 and we used the attenuation values of the testbed in figure 3.8, a `txpower` of 16dBm in T_2 and a `txpower` of 0dBm in T_1. The link budget for $T_2 \rightarrow R_2$ when set to channel 56 results in an SINR value at R_1 near 4 dB (verified with the spectrum analyzer). This value verifies our ξ calculations and is below the minimum one in table 3.3. Despite this, we see in table 3.4 that the $T_1 \rightarrow R_1$ link manages to push data through at all rates and one can notice that as the rate goes higher the drop in throughput increases. This can be attributed to an increase in the Bit Error Rate (BER) as the rate increases. The fact that the rate of 24Mbps achieves the best throughput can be attributed to synchronization issues of the two links, which occurs at the high utilization of the $T_2 \rightarrow R_2$ link. As one can see in figure 3.10 the interfering channel utilization is of critical importance to the resulting throughput as in this testbed our interference is patterned according to the 802.11a DCF.

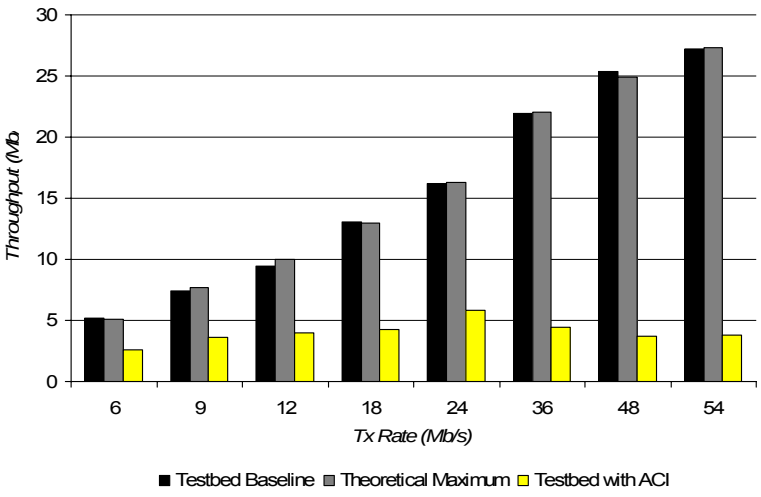

Figure 3.9: *Throughput in link T1→R1 for 1470 bytes payload with- and without ACI.*

TABLE 3.4
ACI EFFECT IN THROUGHPUT (IN Mb/S) FOR HIGH UTILIZATION IN THE ADJACENT CHANNEL WHEN ONLY THE PACKET CAPTURE MECHANISM IS AFFECTED

Tx Rate (*Mbps*)	Without ACI			With ACI		
	udp payload (*bytes*)					
	1470	**1000**	**500**	**1470**	**1000**	**500**
6	5.3	4.9	4.1	2.7	2.6	2.2
9	7.4	6.9	5.7	3.7	3.2	2.5
12	9.4	8.8	7.0	4.0	3.9	3.0
18	13.1	12.0	9.0	4.3	3.7	3.1
24	16.2	14.2	10.2	5.8	4.7	3.7
36	21.9	18.1	12.2	4.4	4.7	2.6
48	25.4	21.3	13.8	3.7	3.1	2.2
54	27.2	22.1	14.1	3. 8	3.2	2.2

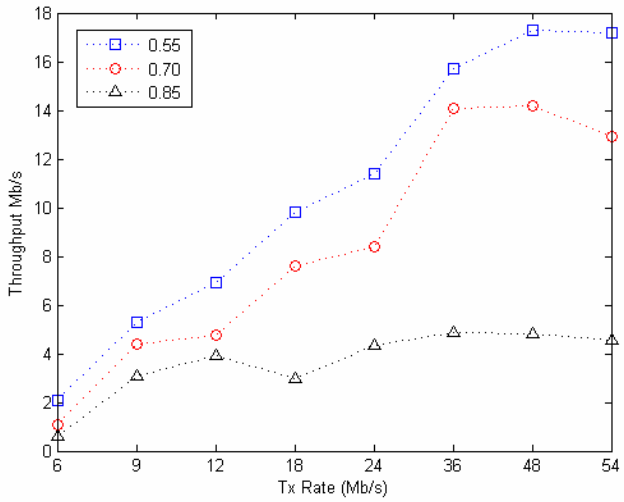

Figure 3.10: *Throughput in link T1→R1 for 1470 bytes payload with 802.11a ACI at the next channel, with a utilization of 0.55, 0.7, 0.85*

B. *LINK BUGET EXTENSION TO INCLUDE DIRECTIONAL ANTENNAS*

Having gained valuable experience from the indoors testbed, we decided to examine how the real wireless medium would behave in a controlled and comparable

setup. We therefore removed the cables from the testbed and conducted the next set of experiments on the roofs of the buildings of the FORTH campus.

We employed two types of antennas: Interline's 19dBi patch panels and Vesuvius Streamline's 27dBi patch panels. We also used mmcx-to-N pigtails and 5m long N-to-N terminated LMR-400 extension cables to physically separate the antennas (see example 3.1). The antennas were mounted on tripods on one end of the links and on a 1.7m tall 3m wide post on the other. Figure 3.11a is an on-site photo of the post, with two of the 27dBi antennas mounted on it; Figure 3.11b is a photo of the tripods with the 19dBi antenna panels during the initial calibration measurements. The details for the equipment used in the testbed are summarized back in table 3.3 above.

The goal of our experiments was to examine the applicability of the ACI model presented, at the near end of a multi-radio node with directional antennas in outdoors environments, since we had already verified its applicability on the laboratory wireless emulation testbed, where cables and attenuators emulated the wireless medium. To this end we had to extend the interference budget calculation in order to account for the radiation patterns directional antennas.

(a) (b)

Figure 3.11: *The testbed setup for the outdoors experiments (a) with 27dBi patch panel antennas on the post, (b) with 19dBi patch panel antennas on tripods.*

Adapting the interference budget calculation of eq.(3.5) to account for directional antennas requires the radiation pattern of the antennas used. One has to find the relative gains along direct line connecting the two nodes, as in figure 3.12. Once this is done the interference budget of eq.(3.5) can be rewritten as:

$$B_{1\to 2} = TxPower + \xi_{1,2} + GantTx(\theta_1) + GantRx(\theta_2) + PathLoss(Tx1 \to Rx2) \quad (3.10)$$

This interference budget is the first expression to our knowledge which accounts for both adjacent channel interference and directional antenna gains. Its importance lies in the fact that it can be used in multi-radio systems to (a) predict if the CCA mechanism will give false positives and (b) calculate the interference at a receiver by transmitting radio-interfaces of the same node, therefore calculate the effective SINR at a receiver..

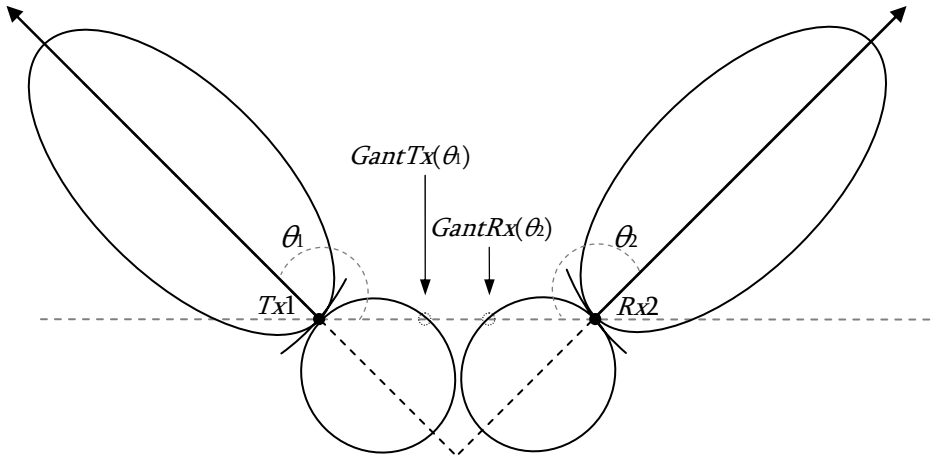

Figure 3.12: *Calculation of the Antenna Gain factors for non-aligned antennas from their radiation patterns.*

The wireless testbed was set up on the roofs of two buildings 250m apart in the campus of FORTH (see Fig. 3.13), at a height of 10m above ground, with a

Fresnel zone clearance[8] of approximately 8m. Significant portion of the path between the two buildings is above the parking lot of FORTH. The majority of the experiments were conducted during weekends and therefore the lot was practically empty. For validation and completeness purposes we performed a few tests with a full parking lot, and as it can be seen from the results the variation was insignificant

Figure 3.13: *A view of the tests paths from Google Earth*

Two parallel links were established between the two buildings. The antenna separation at the ends of the links was either 1.5m or 3m. The antennas used were either 19dBi, or the 27dBi patch panels on all four nodes,. The transmit powers used were either 1dBm or 10dBm. The basic rate was again locked at 6Mbps.

With these parameters we tested how one of the links would perform in terms of throughput, under interference generated mainly on one of the end nodes, from either the immediately adjacent 802.11a channel or from the next

[8] The first Fresnel zone for 250m at 5.3GHz (channel 60) is 2m,

adjacent channel; typically we would run the test on a link in channel 60 and the interferer would be in adjacent channel 56 or next adjacent channel 52. The interfering link was in all cases fixed at the rate of 6Mbps, and would start first generating UDP traffic with full, 1470 bytes, payload packets thus producing the maximum possible 802.11a channel utilization of approximately 90%. A key difference from the indoor testbed is that the "interfering" link would suffer the same ACI effects from the test link leakage.

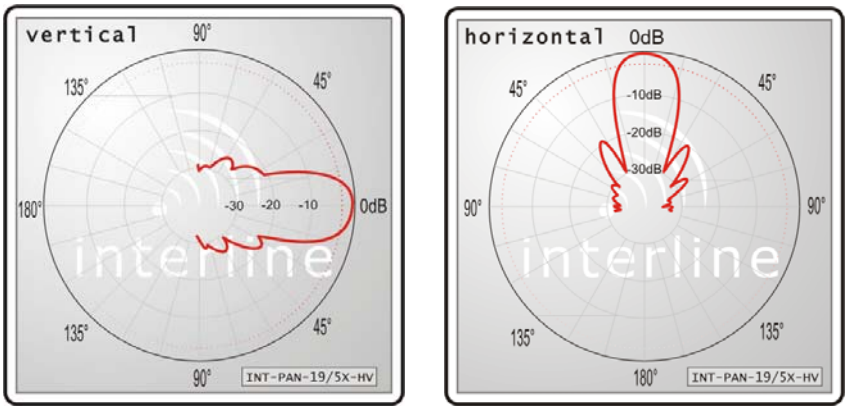

Figure 3.14: *The radiation patterns for the interline antennas used provided by the vendor.*

The test process was the following: the test link would generate a 30sec UDP flow for each rate supported by the 802.11a, for 3 payload sizes: 500, 1000 and 1470 bytes, under the influence of the interferer which had begun generating traffic, as described above, 5 seconds before the test link was activated and continued for 5 seconds more after the test link had finished its transfer. For stability and reproducibility purposes we would unload and reload the MadWifi driver with the new rate parameter for each run. To this end the entire process was shell-scripted and so each test of the link resulted in a run-time of approximately 45 minutes due to more synchronization and other loading/unloading overheads. In all cases a single run of the test link alone, without the activation of the interferer, was conducted to set the baseline performance.

According to the specifications of the antennas, the front-to-back ratio is at least 25 dB in the 19dBi patches and at least 35 dB in the 27dBi case. Incomplete radiation patterns are provided by the vendors (as in figure 3.13), but since the antennas were placed in parallel we required only the +/-90^{o} gain values (for the *GantTx*(90^{o}) *and GantRx*(-90^{o}) of eq.(3.10)).

The tests were designed with power, and distance setting resulting from calculations using eq.(3.10), for the given antennas The path loss model was assumed to be the one of eq.(3.8). The purpose was to examine how one interface will be affected due to ACI caused by another interface on a multi-radio node equipped with directional antennas. In the previous section we identified the two mechanisms that are affected due to radio ACI: (i) The correct data reception and (ii) the Clear Channel Assessment of 802.11a. The first is a PHY layer mechanism and reduces goodput by increasing the packet error rate at the receiver, while the second is a MAC mechanism that results in a transmitter falsely deferring during the 802.11a DCF and thus again goodput reduction. Two major classes, based on fig.3.3 and fig.3.4, of tests were performed in order to look into the two mechanisms: The first was conducted with the receiver of the test link in the same locale with the transmitter of the interfering link, while in the second the transmitters of both links were collocated. A final set of interference and link budget calculations had been performed to ensure that only the near-end ACI is significant.

Conducting the early stages of the experiment we noticed that our model was not able to accurately estimate the results. To narrow down the fault factors, we tested the real values of received ACI power, using measurements from our monitoring tools. For this we used the Airmagnet Laptop analyzer, to get the per packet received signal power, for the interfering packets, at the testbed we had

set up. We noticed that the measured value would significantly vary from the predicted through the budget model used.

This misestimation was attributed to four possible sources: First the output power of the wireless interfaces was actually not the one issued to and reported by the MadWifi driver. Specifically setting the `txpower` option to 10 dBm, would make the card transmit at a power of approximately 15 dBm, while 1 dBm at the driver, would produce an output power of about 12 dBm. These values were obtained with our spectrum analyzer and a complete matching of driver-controlled transmit power to actual measured transmit powers was conducted in [Ma'08]. Another issue regarding the transmit power is that the values we observed using the spectrum analyzer and that the author of [Ma'08] reports are the maximum values Using the Airmagnet Laptop Analyzer, which reports the signal strength per captured packet, we observed that there were more than one power levels, in a range over 10 dB, used by the interface when a single transmit power was selected by the driver.

Second, we had calculated the physical separation of the antennas to be in their far field and in doing so we had expected the radiation patterns (e.g. of figure 3.12) provided by the vendors to hold. Taking the per packet received signal power we discovered that the far field calculation using the Fraunhoffer distance [R'08] was inaccurate, given the radiation patterns of both antennas, was inaccurate. In such a case neither the path loss equation eq.(3.8), nor the radiation pattern should be used in the calculations of eq.(3.11), but rather the actual measured values.

Third, the ACI produced by an 802.11a interface is not a signal of constant power over time since depending on the transmitted data only the active OFDM subcarriers will have variable amplitudes. Hence the assumption that it can be approximated as AWGN is very rough for the calculated SNR.

Finally although we were indicating one of the links as the test link and the other as the interfering link, the process of interference was symmetric: the test link would be interfering with the data transmissions of the interference link since the values of transmitting powers were similar. This is especially reflected on the fact that the results are not highly correlated with the ones of the previous section, where the interference link would not be harmed by the test link.

Following, in all figures we present mean values of goodput obtained over the runtime of the tests. We have a baseline run for a single link at channel 60. In figure 3.15 the antennas attached to the nodes were the 19dBi panels and the txpower was set to 10dBm, producing a 15dBm output, as mentioned above. As we can see an antenna separation by 3m is producing results close to the baseline, even when the transmit power of the interfering link is high and the channels used are immediately adjacent. On the other hand 1.5m is not a sufficient special separation for the ACI to fade over, so it reduces the SNR at the receiver increasing the PER and so reducing the effective throughput. Reducing the transmission power to 1dBm (a real reduction of 3 dB) results in very small PER.

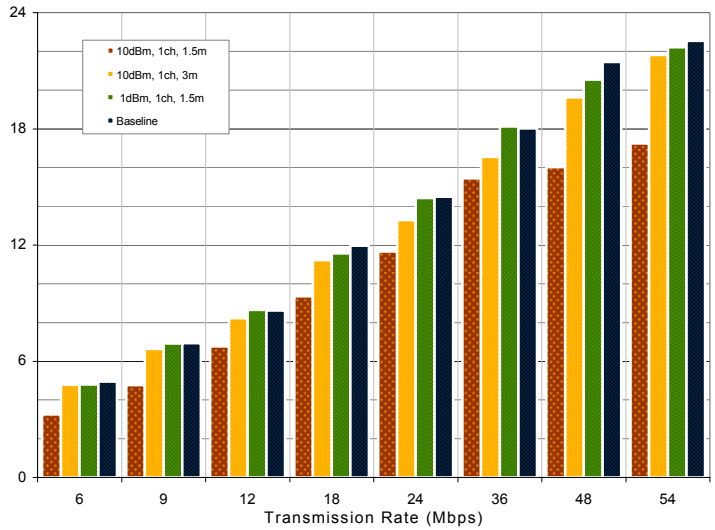

Figure 3.15: *Physical distance of interfering antennas and power effects on the packet capture mechanism for the antennas of 19dBi gain. Effective throughput vs. transmission rate.*

In figure 3.16, we show that using a second interface, at 2 channels away produces no significant ACI as the perceived throughput practically equals the baseline case. Using higher gain antennas results in overcoming the ACI effect due to better beam-forming that allows less power to leak in angles outside the main lobe. This can be clearly seen comparing the 19dBi to 27dBi bars.

Finally figure 3.17, illustrates the effect of ACI on the CCA mechanism for three different packet sizes which correspond to three different channel utilization values. We see that in the low utilization scenario the CCA mechanism is affected the most and regardless of the channel separation. Higher utilizations are more robust and this can be attributed to the symmetrical nature of the interference produced in the testbed (interferer's throughput/utilization is also affected).

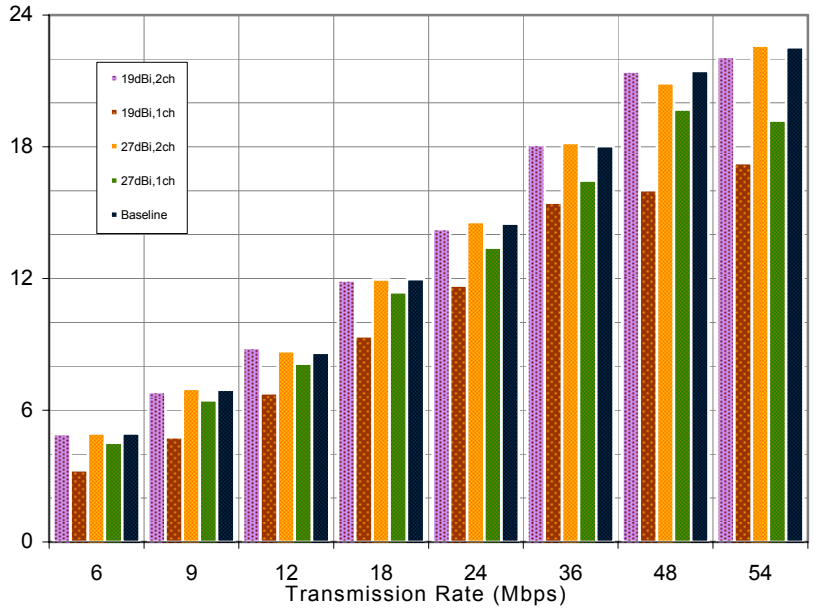

Figure 3.16: *Distance of interfering channel and antenna gain effects on the the packet capture mechanism, for txpower of 10dBm and antennas at 3m apart. Effective throughput for a payload in the UDP flow of the test link set to 1000Bytes.*

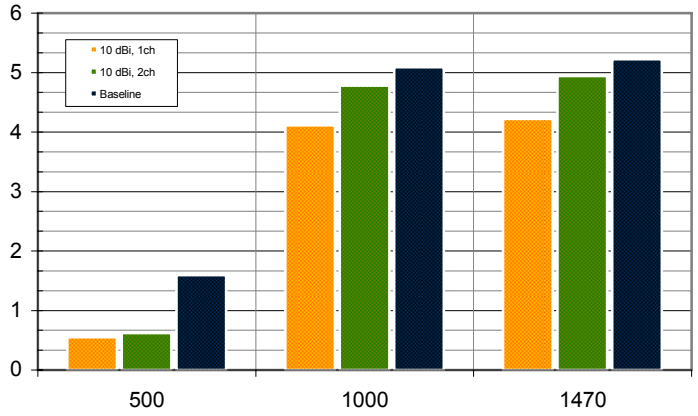

Figure 3.17: *Effect of ACI on the CCA mechanism as it reflect on the effective throughput, versus the packet payload in bytes, for the 6Mbps rate with 19dBi antennas separated by 3m.*

3.4 CONCLUSION

In this chapter we proposed[9] a simple model for quantifying the adjacent channel interference (ACI) power, assuming it can be modeled as constant noise. Unlike [MSBA'06], we verified the model by applying it to off-the shelf IEEE 802.11a radio interfaces. The proposed model of eq.(3.4) was tested and found accurate through measurements with a spectrum analyzer. We identified the two PHY and MAC layer mechanisms that can cause throughput degradation in 802.11a due to false-positives in the CCA assessment and insufficient SINR for data reception at a given rate & BER. Unlike the popularly held belief that 802.11a channels are orthogonal, we identified that the interference power produced by neighboring channels in 802.11a can by harmful for efficient communication.

In order to establish our claim more rigidly, we used our model of ACI power calculation to test an interference budget model in a laboratory testbed and an outdoors testbed. The laboratory testbed was designed to emulate the

[9] concurrently with [MSBA'06].

wireless medium over cables, attenuators and splitters/combiners. The results indicated that although the instantaneous ACI calculation of eq.(3.4) was accurate, the assumption of constant noise modeling would not apply for devices that adhere the 802.11a Distributed Coordination Function. Thus using the proposed model one can predict an instantaneous transmission rate with which data will be received at the 802.11a PER of 10% for 1000 bytes packets under ACI but not long-term throughput. In order to calculate long-term throughput a more accurate model of the 802.11a OFDM transmission should be used rather than the power envelope we used with the spectral mask, when calculating interference.

Still, with this testbed, under these assumptions, we provided real evidence that in 802.11a ACI exists and not only the immediately adjacent but also the next adjacent channels and can significantly degrade the resulting throughput.

Our theoretical modeling is important as it can provide us with worse case scenarios and upper bounds. An interesting application scenario is that of multi-radio nodes such as mesh nodes. Examining how to build a tool for the optimal design of such nodes under realistic constraints for links requirements, antennas to be used and area of deployment, we investigated how our model could be applied a in more realistic outdoors medium-range wireless testbed. The results obtained by this testbed indicated that coupling our model with other models (antenna radiation pattern model & signal propagation loss model) is a delicate process that can introduce errors cannot be attributed to a single source.

In order to be able to alleviate such errors a calibration of the equipment must be performed. Such a calibration procedure is proposed in the end of this dissertation in appendix II.

4

TWO MAXIMAL MATCHING FINDING ALGORITHMS

As we have seen in the previous chapters, given a set of nodes S a matching is a set of simultaneous transmissions from nodes *Ti* to nodes *Ri*. As we have pointed earlier, the matching can be viewed as a one-to-one function of the set of transmitters T onto the set of receivers R. A matching is considered feasible if for all its receivers the SINR criterion is met and this is equivalent to the Perron eigenvalue of matrix F (eq 2.3) being less than 1. Finally a matching is said to be **maximal** if it is feasible and if no link can be added to it and the resulting matching be feasible.

If we are to consider a common SINR threshold θ for all links, then the possible matchings can be partially ordered with respect to the number of links they contain. Finding large, and more so maximal, matchings is important in scheduling. In a case of all links in a potential matching are of equal importance with respect to the quantity of information they will carry during the time the matching will remain active. Thus, larger matchings will manage to push through more information to the destinations, while as we saw in chapter 2 increased matching sizes do not, in general, result in dramatic transmit power increase. On the other hand as we also showed in chapter 2 larger matchings are less likely to be feasible.

Finding all feasible matchings in order to select the largest ones from a set of N possible links is a problem that involves the enumeration of all the

subsets of a set of the N links; that is the enumeration of 2^N items. Verifying the feasibility of matchings is a process that though polynomial, is still quite expensive from a computational point of view, since for a matching of size k, that is a matching having k links, the calculation of the Perron eigenvalue of a matrix $k \times k$ is required which is an operation that costs $O((k \times k)^3) = O(k^6)$.

4.1 MOTIVATION FOR EFFICIENT ALGORITHMS

The key observations for designing algorithms to search for maximal matchings are the following:

a. The cost for checking the feasibility of a 2×2 matching is very low since a 2×2 matrix $X = \begin{bmatrix} a & b \\ c & d \end{bmatrix}$, with a, b, c, d non-negative, has a Perron eigenvalue that is: $(a+d) + \frac{1}{2}\sqrt{(a+d)^2 - 4(a \cdot d - b \cdot c)}$. In the case of an F matrix as in eq.(2.3) where $a = d = 0$ the Perron eigenvalue costs the mere calculation of $2\sqrt{(b \cdot c)}$. Therefore one could start by calculating the feasibility for all possible 2×2 matching of N links and still perform relatively few operations. The gain from this comes when we take into account that:

b. An infeasible matching cannot be subset (**sub-matching**) of a feasible matching –Or equivalently: all matchings which are supersets (**super-matchings)** of an infeasible matching are infeasible [B'04].

Example (4.1):

Assume we are given a set of 4 transmitters and an equal number of receivers, enumerated as T_i, R_i, for i = 1..4. The communication links required to operate are $i = \{T_i \rightarrow R_i\}$ for i = 1..4. The **full matching** would be the set {1,2,3,4}, while

all subsets of this set are all the possible matchings. Now, if the matching {1,2} is shown to be infeasible, meaning that links denoted 1 and 2 cannot be simultaneously activated, then this readily implies that all possible supersets of {1,2} -that is all its super-matchings up to the full matching cannot be feasible: any matching containing links 1 and 2 cannot be feasible since they cannot be simultaneously activated.

Let us examine the reduction in the search space caused by such a single 2×2 infeasible matching, for a set of N possible links. First of all there are matchings of N possible sizes[10]. For any k links, there are $\binom{N}{k}$ matchings. Now, assuming only a single pair of links cannot be concurrently activated then in order to find how many of its super-matchings will be rendered infeasible by it, we consider that fixing these two links in larger matchings would be equivalent to having $N-2$ available links to choose from in order to fill $k-2$ positions for a matching of size k. These are the super-matchings of size k of the infeasible matching. Therefore at each matching size k the number of infeasible matchings due to this single initial infeasible pair is $\binom{N-2}{k-2}$.

We see that this single 2×2 infeasible matching reduces the exponential-sized search space by another significantly large exponential value –since summing the above combinations over the number of places to occupy (here k -2) gives exponential with exponent the items (here N - 2):

[10] If there is at least one 2×2 feasible matching then we do not go into the trivial case of $N=1$. It can, in any case, be assumed that all trivial matchings of $N=1$ are feasible, as long as we do not consider power to be bounded.

$\sum_{k=2}^{N-2} \binom{N-2}{k-2} = 2^{N-2}$. This still keeps the problem in the exponential regime, but the space reduction achieved even in this simple case is: $2^{N-2}/2^N = 1/4$.

In order to appreciate this propagation of infeasibility to super-matchings and the resulting reduction of the search space let us examine a few realistic, with respect to chapter 2, values presented table 4.1. We can readily see that the ratio of infeasible over possible matchings increases with the matching size, and as pointed out in advance the full matching is rendered always infeasible. We therefore move to examine how much computational cost could be gained if we can take advantage of this property and do not calculate the Perron eigenvalue for any of the super-matchings of an infeasible matching.

TABLE 4.1
MATCHINGS RENDERED INFEASIBLE
DUE TO A SINGLE 2×2 INFEASIBLE MATCHING FOR N LINKS

N=	4		6		8	
Matching Size	Possible matchings	Infeasible matchings	Possible matchings	Infeasible matchings	Possible matchings	Infeasible matchings
2	6	**1**	15	**1**	28	**1**
3	4	2	20	4	56	6
4	1	1	15	6	70	15
5	n/a	n/a	6	4	56	20
6	n/a	n/a	1	1	28	15
7	n/a	n/a	n/a	n/a	8	6
8	n/a	n/a	n/a	n/a	1	1

In figure 4.1 we give the ratio of the order of operations required, in order to find all feasible matchings, if the Perron eigenvalue check is not performed for matchings rendered infeasible by the existence of a single infeasible 2×2 matching, over the number of operations required if the exhaustive

solution is followed. We see that for realistic[11] matching sizes of N up to 10, the gain in operations is significantly high.

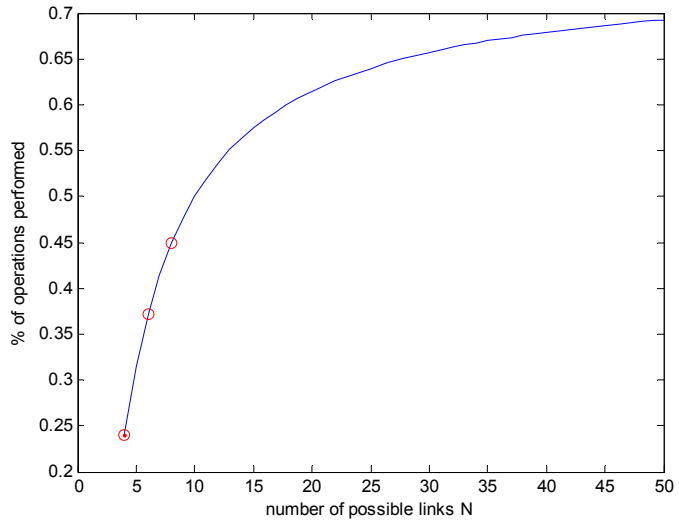

Figure 4.1: *Percentage of operations performed with respect to the exhaustive solution, by looking up on all the sub-matchings feasibility.*

All this suggest that examining the 2×2 matching will be a cheap process that has to be repeated only $\binom{N}{2} = \frac{N(N-1)}{2}$ times. Performing this operation can provide information to significantly reduce the search space, and the search cost. Furthermore, we can expect that some larger-size matchings may be independently found to be infeasible and in a similar fashion further reduce the search space and the computational cost.

Therefore, we can create algorithms that in the general case where some out of the 2^N possible matchings are infeasible, will:

- Probably not need to perform exhaustive feasibility verification for all 2^N possible matchings, but take advantage of the reduction of the search space

[11] With respect to the feasibility probability results of chapter 2.

- Not need to examine for feasibility using the costly Perron eigenvalue, for the majority (table 4.1) of the large possible matchings due to infeasible sub-matchings.
- Guarantee to find at least one maximal matching

4.2. MATCHINGS' STRUCTURING AND ALGORITHMS DESCRIPTIONS

As we saw in the previous section, to gain from infeasibility propagating into super-matchings, we need to structure our data in a way that supports a fast lookup process, since we will be performing up to $O(2^k)$ operations for each matching of k links. To this end, given an ordered set of links, we compose the partially ordered tree-structure as described in table 4.2 and shown in figure 4.2 for the case of $N = 4$.

In our actual implementation we used hash tables to store the tree structure and this may reflect in the description of the algorithms later on. This implementation selection was done primarily because hash tables support fast searching at an average cost of $O(1)$, and because they support fast insertions at a cost of again $O(1)$. The two drawbacks of hash tables namely (i) complicated/expensive hashing functions and (ii) table resizing during insertions are not a concern in our case, since we know that the number of elements to be inserted and we also know they will be representing ordered sets. Hence we could easily construct simple hashing functions that will not be suffer from the known problems that are identified in the literature of data structures and algorithms [CLRS'02, Gg'02].

Algorithm 4.2
CONSTRUCTION OF A TREE OF ALL POSSIBLE MATCHINGS USING A HASH TABLE

Tree_of_Matchings(ordered set of links of size *N*)

1. For *k* = 2 .. *N*
2. Form all $\binom{N}{k}$ sized matchings of *k* links, ordering them based on the link ordering.
3. Initialize each to have ***Feasibility*** := *TRUE*.
4. If (*k* > 2)
5. For each matching of size k,
6. For *i* = 1 .. k
7. **Parent[i]** := { the (k - 1) size sub-matching having
8. all but the (*k* + 1 – *i*)-th element of the current }
9. if (*k* < *N*)
10. For each matching of size *k*,
11. *j* := the ordering of the largest link in the current
12. matching
13. For *i* = (*j* + 1) .. *N*
14. **Child[i-j] :=** { the (k + 1) size super-matching
15. formed as the concatenation of link *i* (next
16. available) to the current matching }.
17. *last_element :=* the ordering of the *k*-th link in
18. the matching
19. If (*last_element* < *N*)
20. **Sibling** := { the matching formed replacing
21. *the last_element* by the next link in the
22. ordering }
23. Else *Sibling* := *null*
24. Store each matching in a hash table with key the ordered elements of the matching and a data structure that contains:
    - a *k*-size table of hash keys *Parent*[],
    - a variable size table of hash keys *Child*[]
    - a key to the right- *Sibling* of the current matching
    - the *Feasibility* of the matching
25. **Return** Hash Table of the Tree Structure

Example 4.2

Assume the number of links is $N = 4$ and that they have been enumerated as 1, 2, 3, 4, and ordered as the numbers used to identify them. We can visualize in figure 4.2 the tree generated by the algorithm of table 4.2 where the lists `Parent`, `Child`, and the `Sibling` of each matching/tree node are represented as directed links towards the matching of the respective hash key(s) stored.

This structure should always be pre-constructed off-line, since the cost for its construction is $O(2^N)$.

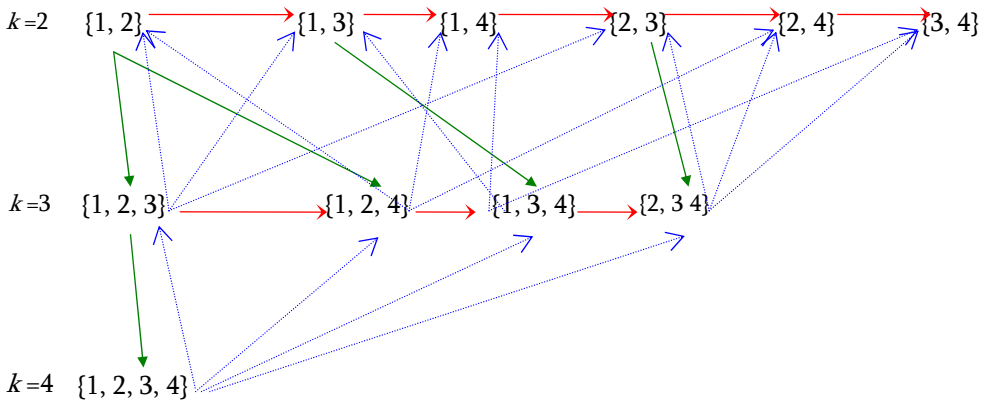

Figure 4.2: *The basic data structure used for building the algorithms. All matchings are stored in a hash table and the directed links shown are lists of keys stored with each matching.*

Given this structure there are simple algorithms to traverse the formed tree based on Breadth- or Depth- first descent. We shall describe a simple Breadth-first fashion search algorithm, and then a Depth-first which falls in the branch-and-bound design category, because of the ordering properties of the tree structure used.

A. Breadth-First based Search

With this algorithm at each tree level all matchings are visited. Computationally we hope to gain using this search method by not having to performing at for some matchings of size k, the $O(k^6)$ operations required for examining feasibility using the Perron eigenvalue. We perform at most k hash table lookups: we examine the matching's parents for feasibility and only when all parents are feasible the calculation of the Perron eigenvalue is performed. The gain is that we are thus reducing $O(k^6)$ to $O(k)$ for each infeasible matching. Due to table 4.1 we expect that this gain will be significantly high even in the case where a single infeasible 2×2 matching exists in the network. Still this is an algorithm of little gain for a large N, since we take advantage only of the feasibility of the parent matchings and not of the virtual reduction of the search space caused by the ordering we created with the tree matchings algorithm. This algorithm will report as maximal the last matching found to be feasible in a complete breadth-first traversal of the tree.

ALGORITHM 4.3

A BREADTH FIRST ALGORITHM FOR MAXIMAL MATCHING FINDING

```
check_Parents'_Feasibility(key, treeLevel)
1. if treeLevel == 1 return True
2. else
3.    for i = 1 .. sizeof (key)
4.          if key→Parent[i]→Feasibility == False
5.          Return False
6.    Return True
```

```
BRMaxMatching(Machings_Tree_Structure, N )

1.    init_key = {1}
2.    for k = 2 .. N
3.          key = {init_key, k}
4.          quick_test := check_Parents'_Feasibility(key)
5.          if quick_test == FALSE
6.                key→Feasibility := FALSE
7.          else
8.                perron = calculate_Perron_Eigenval(key)
9.          if perron >= 1
10.               key→Feasibility := FALSE
11.         else current_Maximal_Matching := key
12.   Return (current_Maximal_Matching)
```

B. Depth-First Branch & Bound algorithm

The algorithm described here takes advantage of the initial key observations of this chapter that help up discard whole branches of the ordered structure created by algorithm `Tree_of_Matchings` of table 4.1 This algorithm can be summarized in the following traversal strategy:

Loop while a new feasible matching is found:

If the current matching is feasible

Then Set this as maximal

Move to examine its first child- super-matching.

Else

Move to examine its first child-bearing sibling for feasibility

We can see that:

- This algorithm will not descend to branches of infeasible matchings thus significantly reducing the search space from the early stages on.
- Performing the feasibility check of a k-sized matching, using check_Parents'_Feasibility recursively, is a key that can save operations at each infeasible matching of size k can reducing the cost of $O(k^6)$ to $O(k^2)$, if the matching had been rendered infeasible due to a parent. This will require to modify line 2 of table 4.2 and initialize the tree so that each node has a `Feasibility := NULL`. Then in order to rewrite a recursive version of the function `check_Parents'_Feasibility(key, k)`, we modify it as in table 4.4 below.

ALGORITHM 4.4
A DEPTH-FIRST BRANCH & BOUND ALGORITHM FOR MAXIMAL MATCHING FINDING

`rec_Check_Parents'_Feasibility(key, treeLevel)`

```
1.  if treeLevel == 1
2.     if calculate_Perron_Eigenval(key) < 1
3.           Return True
4.     else
5.           Return False
6.  else
7.     for i = 1 .. sizeof(key)
8.           if key→Parent[i]→Feasibility == null
9.             neg_result:=rec_Check_Parents'_Feasibility
10.                                (key→Parent[i], treeLevel-1)
11.            if neg_result := False
12.                Return False
13.            else
14.                if calculate_Perron_Eigenval(key) < 1
15.                      Return True
16.                else
17.                      Return False
```

DFMaxMatching(*Machings_Tree_Structure, N*)

```
1.     cur_matching = {1,2}
2.     treeLevel = 2
3.     maximal_matching = cur_matching;
4.
5.     while (1)
6.
7.       if treeLevel == 2
8.         if calculate_Perron_Eigenval(cur_matching) >= 1
9.            cur_matching_is_feasible = False
10.        else
11.           cur_matching_is_feasible = True
12.      else
13.        if rec_Check_Parents'_Feasibility(key, treeLevel) = True
14.          if calculate_Perron_Eigenval(key) >= 1
15.            cur_matching_feasible = False
16.          else
17.            cur_matching_is_feasible == True
18.        else
19.          cur_matching_is_feasible == False
20.
21.      if cur_matching_is_feasible == True
22.          maximal_matching = cur_matching
23.          if treeLevel == N
24.                Return maximal_matching
25.          else
26.                if cur_matching has Child[1]
27.                      cur_matching := Child[1]
28.                      continue
29.                else
30.                      if cur_matching has Sibling
31.                            cur_matching := Sibling
32.                            continue
33.                      else
34.                            Return maximal_matching
35.      else
36.        if cur_matching has Sibling
37.          cur_matching := Sibling
```

```
38.           continue
39.         else
40.           Return maximal_matching
```

We coded the proposed algorithms in MATLAB and we also coded:

- an exhaustive algorithm that would examine all matchings for feasibility by calculating the Perron eigenvalues
- a brute-force algorithm that would begin searching for a maximal matching by examining the largest matchings first, calculating the Perron eigenvalue, that would terminate at the first feasible matching found.

We tested these four algorithms for 3 up to 9 links in order to examine how they would perform in terms of the order of operations performed. Setting for each number of links a requirement for $\theta = 1 / (N - 1)$ common in all links, as in chapter 2, we run the test for 5000 topologies in each case, assuming path loss exponent of $n = 2$. In Figure 4.3 we give the mean of the order of operations to be performed for each of the four algorithms, over the runs. In fig 4.4 we show the empirical PDFs of the order of operations to be performed for the case of $N = 5$ for our two algorithms and for the brute force one. Finally in figure 4.5 we present the respective CDFs which clearly indicate that at least 70% of the samples will perform less than the mean value the order of operations.

As expected the best performing algorithm, is the one with the depth-first branch-and-bound approach, which effectively performs a number of operations of approximately the same order to those that the brute force solution would perform in if the links were fewer by 3.

Looking into figures 4.4 and 4.5 we observe that the expected values are overestimating the bound for the bulk of the samples. This skewness in the expected value can be explained by the heavy tailed PDF that is caused by a significant probability (for all cases we see that it is at about 15%) that some large and costly matching of size close to *N* will be feasible. In such a case we have to pay the very high cost for the maximal matching, regardless of the algorithm followed.

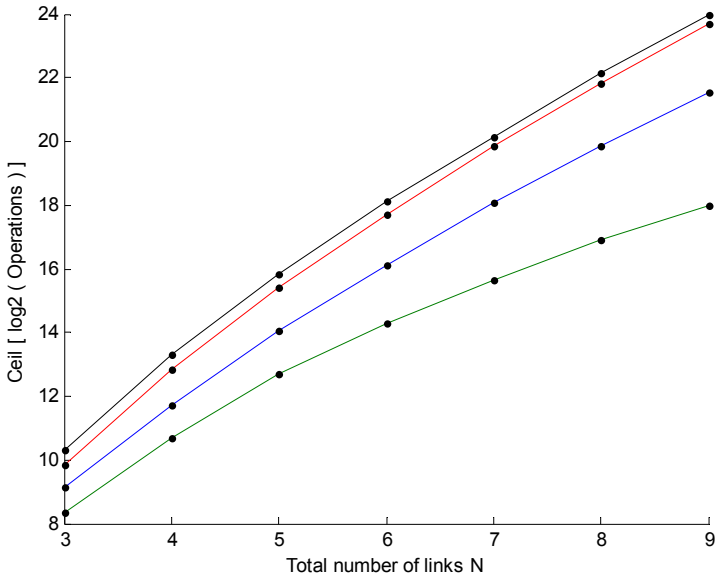

Figure 4.3: *Simulated upper bound of the operations performed for the exhaustive (Black), a Brute-Force (Red), the Breadth-First –Based Search (Blue) and the Depth-First branching algorithm (Green).*

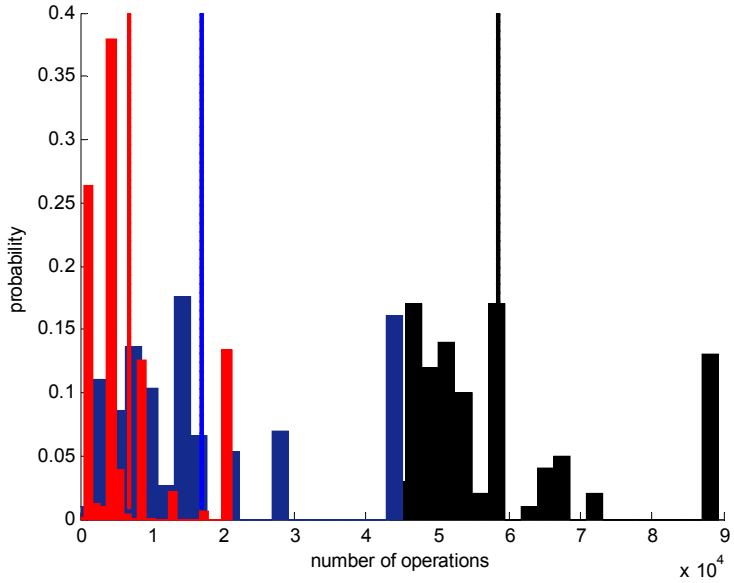

Figure 4.4: *For N=5: empirical probability density functions of the upper bound of the number of the expected operations of the Brute-Force (black), the Breadth-First –Based Search (Blue) and the Depth-First branching algorithm (Red), vertically the respective expected values for each.*

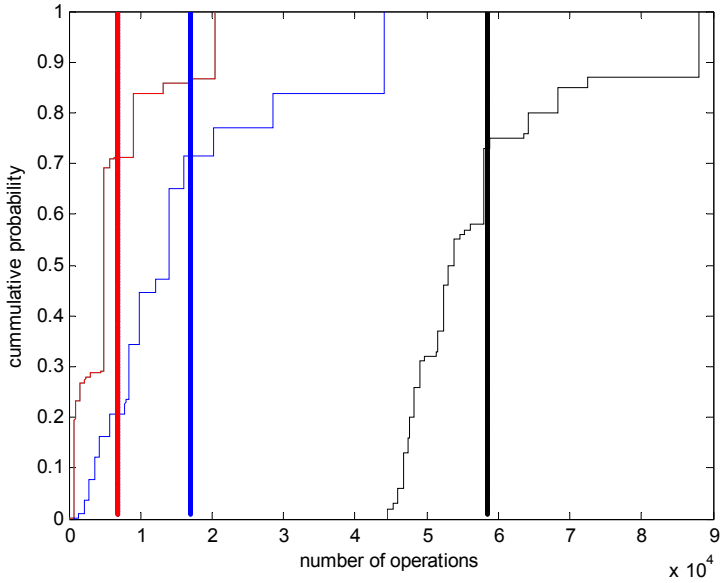

Figure 4.5: For $N = 5$: cumulative density functions of the respective algorithms, *same color coding as in figure. 4.4.*

4.3 CONCLUSION

Finding maximal matchings is an important problem that reflects in scheduling. Although there are stochastic algorithms in the literature [B'04, BE'04] that can produce fast a feasible maximal matching, we were concerned with providing algorithms that deterministically will return a maximal matching. This is a known hard problem. However we showed that constructing off-line a tree structure that holds all the possible matchings taking advantage of the fact that infeasibility propagates in super-matchings, the search space can be effectively reduced.

We provided two algorithms: one that saves operations by taking advantage of the cheaper infeasibility calculations of sub-matchings and another that takes advantage of the search-space reduction. Both in the worse case are exhaustive, still both outperform significantly a brute-force search algorithm and achieve the goal of always providing one maximal matching, as they are based on well-known tree traversal algorithms.

5
DISCUSSION & FUTURE WORK

In this dissertation we presented three topics with impact in the design of ad hoc and mesh networks. The common denominator of all three is the transmission power control that enables node to node communication under given quality of service requirements that are expressed with the SINR criterion.

Initially we presented a thorough study of well-known SINR-based power assignment methods in a wireless ad hoc network. We provided insight for the feasibility probability of a matching with respect to its size, its SINR threshold and the path loss exponent. We also provided structural findings on the properties of the Perron eigenvalue and the sum of the elements of the normalized Perron eigenvector of matrices of the form used in the power assignment solutions for the noiseless and noisy case.

Furthermore, we examined jamming nodes and how they can reduce the aggregate capacity of an interference-limited ad hoc network. We illustrated that even an adaptive network cannot effectively mitigate these jamming attempts, by simply increasing its transmitting powers, under a maximum power constraint. We also established that using more than one jamming nodes does not require more power on the average, thus resulting to longer jammer lifetime, at the cost of having more complex jammer nodes which need to cooperate in order to be able to each use the minimum power to harm the network. Finally we proposed a strategy, to minimize the power cost, for a single jammer with mobility and increased computational capabilities, in order to harm an adaptive network.

We proposed a model to quantify the ACI power. Unlike previous

works, we verified the model by applying it to off-the shelf IEEE 802.11a radio interfaces, which is widely regarded to have orthogonal channels. The proposed model of eq.(3.4) was tested and found accurate through measurements with a spectrum analyzer. We thus concretely established that 802.11a adjacent channels are not orthogonal and so we are able to explain the experimentally observed link degradation. We also identified the two PHY and MAC layer mechanisms that can cause throughput degradation in 802.11a due to false-positives in the CCA assessment and insufficient SINR for data reception at a given rate & BER requirement. With a laboratory testbed we provided the first systematic evidence that a predictable 802.11a ACI exists and not only the immediately adjacent but also the next adjacent channels and significantly degrade the resulting throughput.

Although the instantaneous ACI calculation of eq.(3.4) for 802.11a was accurate, the assumption with which it we could generate constant interference using off-the-shelf devices does not hold, since 802.11a based devices adhere the protocol DCF. Thus using the proposed model one can predict an instantaneous throughput, but not long-term goodput. In order to calculate long-term throughput a more accurate model of the 802.11a OFDM transmission coupled with the 802.11a DCF needs to be developed rather than the one contained here. Our theoretical modeling is still important, as it can provide us with worse case scenarios and upper bounds.

An application scenario for ACI calculation and mitigation is that of mesh multi-radio nodes. Examining how to build a tool for the optimal design of such nodes under realistic constraints for links requirements, antennas to be used and area of deployment, we investigated how our model could be applied in a more realistic outdoors medium-range wireless testbed. The results obtained by this testbed indicated that coupling our model with other models (antenna radiation

pattern model & signal propagation loss model) is a delicate process that can introduce errors which cannot be attributed to a single source. In order to be able to alleviate such errors a calibration of the equipment must be performed. Such a calibration procedure is proposed in the end of this in appendix II.

Finally, dealing with a known computationally hard problem of finding maximal matchings we showed that taking advantage of the fact that infeasibility of matchings propagates in super-matchings, the search space can be effectively reduced. We provided two algorithms: one that saves operations taking advantage of the infeasibility calculations that have been performed in sub-matchings, and another that takes advantage of the search-space reduction. Both in the worse case are exhaustive, still both on average outperform significantly a brute-force search algorithm and achieve the goal of always providing one maximal matching, as they are based on well-known tree traversal algorithms.

APPENDIX I

POWER ASSIGNMENT FOR A TOY-CASE

In this appendix we present the toy problem of a 2×2 matching in order to illustrate the key points of the power assignment methods for a noiseless system [GVG'93] and a system with noise [T'05].

Assume two pairs of transmitters-receivers as in figure A.1., with all path loss G_{ij} values known, operating T_1 and T_2 with the powers P_1, P_2 respectively.

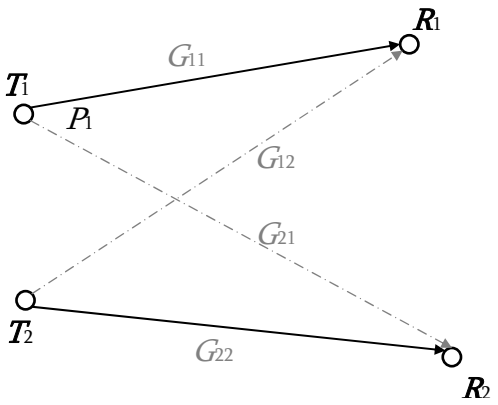

Figure A.1: *The toy problem of finding powers in a 2×2 matching.*

In the noiseless case this will result in the following Signal to interference (SIR) values at receivers R_1 and R_2: $\gamma_1 = \frac{P_1 G_{11}}{P_2 G_{12_1}}$ $\gamma_2 = \frac{P_2 G_{22}}{P_1 G_{21}}$

The authors of [GVG'93] showed that in this case we can answer:

1) Whether we can find a power vector P, such as to maximize the minimum SIR value in the network.
2) If yes, then what would this maximum SIR value be, and

3) Which is that power vector?

The answer lies in the matrix $A = \begin{bmatrix} 0 & \frac{G_{12}}{G_{11}} \\ \frac{G_{21}}{G_{22}} & 0 \end{bmatrix}$, which is non-negative and irreducible, and as such has a real maximum positive eigenvalue ρ_A which is known as the Perron eigenvalue of A. The eigenvector associated with the Perron eigenvalue is known as the Perron eigenvector and is element-wise positive. *Using the Perron eigenvector as a power vector, the SIR becomes equal to $1/\rho_A$ at all receivers and is the maximum of the minimum value.*

If a $\theta = [\theta_1, \theta_2]$ vector of SIR thresholds to be exceeded is given for this system, the power vectors $P = [P_1, P_2]^T$ that achieve: $\frac{P_1 G_{11}}{P_2 G_{12}} \geq \theta_1$ and $\frac{P_2 G_{22}}{P_1 G_{21}} \geq \theta_2$ are the ones lying in the region bounded by the blue lines in figure. A.1.

In the presence of noise the same $\theta = [\theta_1, \theta_2]$ SINR threshold is achieved by all power vectors in the grayed area in figure. A.1, since: both $\frac{P_1 G_{11}}{P_2 G_{12} + N_1} \geq \theta_1$ and $\frac{P_2 G_{22}}{P_1 G_{21} + N_2} \geq \theta_2$ must hold.

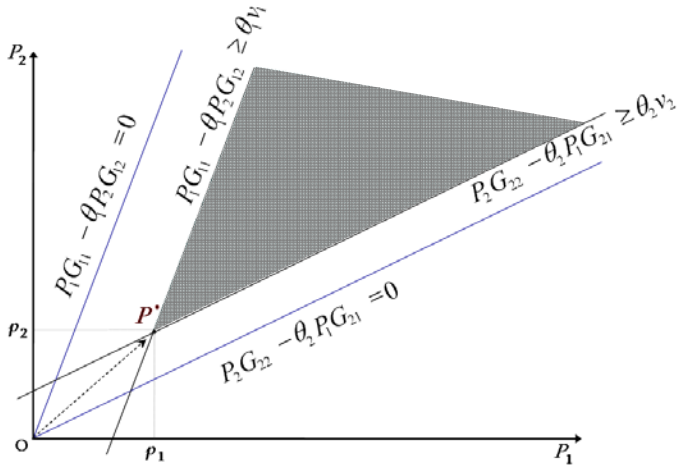

Figure A.2: *The power feasibility region for the toy problem of figA.1 in the noise-less .(Blue) and in the noisy (Gray) cases.*

APPENDIX II

CALIBRATING MULTI-RADIO NODE COMPONENTS

As we saw throughout Chapter 3 ACI generated by nearby transmitters can significantly degrade the resulting throughput of wireless interface. Therefore, based on eq.3.11 we could build a software tool that will determine for a muti-radio node:

(i) what antennas should be used in order to establish required point-to-point links

(ii) how these antennas should be placed in relation to each other, in order to minimize near-end interference and

(iii) with what power to transmit from each of the radio-interfaces,

such that maximum uplink and downlink throughput can be achieved aggregately for all predetermined links, under the constraint that: All interfaces should achieve a minimum, uplink and downlink throughput. Realistic assumptions that can be made are that:

(i) the selection pool of available antennas is limited

(ii) the selection pool of transmission powers is limited

(iii) the SINR requirements are known for each transmission rate

In the previous section we identified that the key points of failure of equation 3.11 in the real world were:

(i) the path loss calculation model used

(ii) the antenna radiation pattern data provided by its vendor

(iii) the reported transmit power errors

along with any other hidden/unreported vendor/driver optimizations at the wireless radio interfaces used such as spectral masks that are better that the protocol requirement.

These can be alleviated by a calibration procedure of the available equipment before any calculations. We shall describe how to perform with sufficient accuracy for 802.11a/g devices, such a procedure without using specialized equipment. We will require:

- a wireless network monitoring tool which can accurately obtain the signal strength of each received packet [AM'08, K'08]
- a single fixed attenuator of high loss

-STEP 1: *Verifying the transmit power of the available interface*

We connect a test node with the monitoring tool using the same radio interface on both nodes, using the fixed attenuator. The high fixed attenuator must be used so that the maximum input power is not exceeded at the receiver.

For each transmit power, at each supported data rate we must transmit a large number of packets with random payloads from the test node to the monitoring node. We record the received signal strength for each transmission. We expect that all data packets should be received at the same power. If that is the case then we can calculate the actual transmission power corresponding to the driver-reported transmission power and data rate as the received power by subtracting the value of the attenuator used along with the attenuation caused by interconnecting cables and connectors. Otherwise, if different power levels are observed, as mentioned above, which may be happening due to adaptive power control, or cell breathing techniques used, without these being reported in data sheets, we

must record a long sample of packet powers in order to find how many power levels there are and with what probability is each used.

The reason for performing this calibration at each data rate is that different data rates are achieved by different modulation techniques which results to different output power requirements for different constellation symbols and this may lead to different transmission powers. For extra scrutiny this test can be performed on more than one channel in order to establish if the measured values hold over all the available channels. This may not be the case if the interface tunes poorly on some channels.

-STEP 2: *Verifying antenna Patterns and Gain values*

Having established the real transmission power (be it a single one or a random variable) for all data rates we connect each of the antennas on the interface of the monitoring node and perform measurements to establish the relative antenna gain at various angles off the main lobe.

A simple process that can be followed is to connect two identical antennas on two interfaces and set up a point to point link at an outdoor wide-open area. The received signal power in that case will be:

$$R = TxPower + 2Gant + PathLoss(\mathrm{d}) \tag{3.9}$$

where all values, as in eq.(3.5), are expressed in dB.

As in the previous step we record the values of R for a many data transfers in order to smooth-out fluctuations of the *PathLoss* factor, since now we are in the real wireless medium. In order to verify the provided antenna pattern we have to rotate the antenna attached to the monitoring node to some of the interesting points of the pattern. Begin by examining the rotation by 180^{o} in order to establish whether the Front-to-Back ratio is correct. Performing the per packet

power measurements as before, having changed only one antenna orientation, will result in receiving a power at:

$$R' = TxPower + 2Gant + FtoB + PathLoss(\mathrm{d}) \quad (3.10)$$

As we can see, the result of subtracting R from R' should be the equal to the Front-to-Back ratio, so we can establish whether the reported Front-to-Back ratio is correct and in the same manner we verify at more points of interest on the pattern such as the side-lobe peaks and the pattern minima. One last measurement must be taken to quantify the cross-polarization loss.

Again this process should be repeated for more than one channel as the antenna pattern and the cross-polarization loss may vary when tuning to different frequencies. This can be performed easily since whenever the antenna is set to an angle of interest the measurement of R' can be performed in a scripted fashion over all available channels.

Finally, since we assumed to have a given, typically small pool of antennas this process could be used to verify the relative gains reported by the antennas: Having performed a baseline measurement of R with the setup used in eq.(3.9), instead of tilting one antenna, exchange it with another from the pool.

-STEP 3: *Estimating the path losses*

There is need to estimate two path losses: the one of the near-end interference paths and the one of the communication links we aim to establish. The latter requires a single set of on-site measurements using known transmit powers and calibrated antennas. The latter, being susceptible to reflections and diffractions caused by signals generated nearby will be extremely hard to estimate and accurately fit to a simple path loss model. Therefore, for the sake of simplicity another on-site measurement can be performed as before and using eq.(3.10) retrieve a sample of the near-end path loss random variable for a single interference path.

Quantizing this sample to three values we can characterize this link to having low, medium and high path loss, and from those we can find the best-fitting path loss exponent for each case using eq.(2.1). Hence we propose to use a 3-level estimate of the path loss based on the interference path distance. The idea behind this simple modeling is that we can generate the design tool to initially handle the lowest estimated path loss and if no solution can be found then relax it.

REFERENCES

[802.11'99] IEEE 802.11, Wireless LAN Medium Access Control (MAC) and Physical Layer (PHY) Specifications, Standard, IEEE, August 1999.

[802.11a'99] IEEE 802.11a, Part 11: Wireless LAN, Medium Access Control (MAC) and Physical Layer (PHY) Specifications: High-Speed Physical Layer in the 5 GHz Band, supplement to IEEE 802.11 Standard, September 1999.

[802.11h'03] IEEE 802.11a, Part 11: Wireless LAN, Medium Access Control (MAC) and Physical Layer (PHY) Specifications Amendment 5: Spectrum and Transmit Power Management Extensions in the 5 GHz band in Europe, October 2003.

[AM'08] AirMagnet Laptop Analyzer, online at: http://www.airmagnet.com/products/laptop_analyzer/

[APKST'08] V.Angelakis, S.Papadakis, N.Kossifidis, V.Siris and ATraganitis "*The Effect of Using Directional Antennas on Adjacent Channel Interference in 802.11a: Modeling and Experience With an Outdoors Testbed*", 4th International workshop on Wireless Network Measurements, (WiNMee 2008), Berlin, Germany, March , 2008.

[APST'08] V. Angelakis, S. Papadakis, V. Siris and A. Traganitis, "*Adjacent Channel Interference in 802.11a: Modeling and Testbed validation*", 2008 IEEE Radio and Wireless Symposium, Orlando, FL, USA, Jan. 2008.

[AS++'07] V.Angelakis, V. Siris, et. al. "*Heraklion MESH: An Experimental Metropolitan Multi-Radio Mesh Network*" WiNTECH'07, Montréal, Québec, Canada, Sept., 2007.

[ATS'07] V. Angelakis, A. Traganitis, V. Siris, "*Adjacent channel interference in a multi-radio wireless mesh node with 802.11a/g Interfaces*", IEEE INFOCOM 2007, Anchorage, AL, USA, May 2007.

[AWMN'08] Athens Wireless Metopolitan Network, online at: http://www.awmn.net/

[AWW'05] I.F. Akyildiz, X. Wang, W. Wang, "*Wireless mesh networks: a survey"* Computer Networks, Volume 47 Issue 4, 15 March 2005, p.445-487.

[B'04] S. A. Borbash, Design Considerations in Wireless Sensor Networks, Ph.D. Thesis, Institute of Systems Research, University of Maryland, 2004.

[BCG'05] R. Bruno, M. Conti, E. Gregori, "*Mesh networks: commodity multihop ad hoc networks"*, IEEE Communications Magazine, Volume 43, Issue 3, March 2005, p.123-131

[BE'04] S. A. Borbash, A. Ephremides. "*The feasibility of matchings in a wireless network*", In Proc. Intl. Symp. Information Theory, 2004

[BE'06] Steven A. Borbash, Anthony Ephremides, "*Wireless Link Scheduling With Power Control and SINR Constraints*". IEEE Transactions on Information Theory, vol52 nr.11, 2006.

[C'08] Cisco Aironet 1200 Series Access Point Data Sheet, available online at: http://www.cisco.com/en/US/prod/collateral/wireless//ps5678/ps430/ps4076/ /product_data_sheet09186a00800937a6.pdf

[CCL'03] I. Chlamtac, M. Conti, and J. Liu, "*Mobile Ad Hoc Networking: Imperatives and Challenges*," Ad Hoc Networks, vol. 1, no. 1, , pp. 13–64, July 2003.

[CHKV'06] C. M. Cheng, P. H. Hsiao, H. T. Kung, and D. Vlah, "*Adjacent Channel Interference in Dual-radio 802.11 Nodes and Its Impact on Multi-hop Networking*", IEEE GLOBECOM 2006, San Francisco, CA, USA, Nov. 2006.

[CLRS'02] T.H. Cormen, C.E.Leiserson, R.L. Rivest, and C. Stein, Introduction to Algo rithms, McGraw-Hill, 2002.

[EAT'06] A. Ephremides, V. Angelakis and A. Traganitis, "*SINR Ad hoc Networking*", proceedings of 17th IEEE Symposium on Personal, Indoor and Mobile Radio Communications (PIMRC'06), Helsinki, Finland, September 2006

[FM'93] G. J. Foschini and Z. Miljanic, "*A simple distributed autonomous power control algorithm and itsconvergence*" IEEE Trans. Veh. Tech., vol. 42, no. 4, pp. 641–646, Apr. 1993.

[Ga'64] F.R. Gantmacher, Matrix theory, 3rd ed. Chelsea publishing, USA, 1964

[Gg'02] G.F. Georgakopoulos, Data Structures, Crete University Press, Greece, 2002

[GK'00] P. Gupta and P. R. Kumar. "*The Capacity of Wireless Networks*" IEEE Trans. on Information Theory, 46(2):388–404, March 2000

[GVGZ'93] S. Grandhi, R. Vijayan, D Goodman, J. Zander, "Centralized power control in cellular radio systems". IEEE Transactions on Vehicular Technology, 42(4):466-468, 1993.

[H'05] M. Haenggi, "*On Distances in Uniformly Random Networks*", IEEE Trans. on Information Theory, vol. 51, pp. 3584-3586, Oct. 2005.

[HGG'03] T. Holliday, A. Goldsmith, and P. Glynn, "*Distributed Power Control for Time Varying Wireless Networks: Optimality and Convergence*", Proceedings: Aller ton Conference on Communications, Control, and Computing, Monticello, IL, Oct. 2003

[HJ'91] R. A. Horn and C. R. Johnson, Topics in Matrix Analysis, Cambridge University Press, Cambridge, U.K.1991.

[HWMN'08] Heraklion Student Wireless Network, online at: http://wireless.uoc.gr/smf/

[I'08] Interline Antennas, online at: http://www.interline.pl/html/modules/content/index.php?id=2&lang=english

[JE'02] Jung Jee and Hossain Pezeshki Esfahani. "*Understaning wireless LAN Performance Trade-Offs*". Communications Systems Design Nov. 2002. Online at: http://img. cmpnet.com /commsdesign/csd/ 2002/nov02/feat3-nov02.pdf

[JPPQ'05] K.Jain J.Padhye V.Padmanabha L. Qiu, "*Impact of Interference on Multi-Hop Wireless Network Performance*", Wireless Networks 11, 471–487, 2005

[JPS'03] Jun J., Peddabachagari P., Sichitiu M. "*Theoretical Maximum Throughput of IEEE 802.11 and its Applications*", IEEE NCA'03, Cambridge MA., USA, Apr. 2003.

[K'08] Kismet, available online at: http://www.kismetwireless.net

[KGV'83] S. Kirkpatrick, C. D. Gelatt and M. P. Vecchi, "*Optimization by Simulated Annealing*", Science, Vol 220, Number 4598, pages 671-680, 1983

[KN'05] M. Kodialam, T. Nandagopal, "*Characterizing achievable rates in multi-hop wireless mesh networks with orthogonal channels*", IEEE/ACM Transactions on Networking (TON) archive Vol.13,4 868-880, Aug.2005

[KK'05] V. Kawadia and P. R. Kumar, "*Principles and Protocols for Power Control in Wireless Ad Hoc Networks*", IEEE Journal on Selected areas in communications Vol. 23,1, Jan. 2005.

[KK'03] V. Kawadia and P. R. Kumar, "*Power control and clustering in ad hoc networks*".InfoCom 2003, San Francisco CA. USA, April, 2003

[LYCZ'06] Jian Liu , Dongfeng Yuan, Song Ci and Yingji Zhong, "*Nonlinear optimization for energy efficiency in IEEE 802.11a wireless LANs*", Computer Communications, Volume 29, Issue 17, 8 November 2006, p.p. 3455-3466.

[M'08] MadWifi, online at: http://madwifi.org/wiki/About

[Ma'08] K.I. Mathioudakis, Monitoring System and performance measurement of Wireless Metropolitan Area Network, M.Sc Thesis, Compure Sciecne Dept., University of Crete, Greece, 2008.

[MSBA'06] A. Mishra, V. Shrivastava, S. Banerjee, W. Arbaugh, "*Partially Overlapped Channels Not Considered Harmful*", SIGMetrics/Performance'06, Saint Malo, France, Jun., 2006.

[PBO'07] F. Potorti, P. Barsocchi and G. Oligeri "*Frame error model in rural Wi-Fi networks*", WiNMee 2007, Limassol, Cyprus, Apr. 2007.

[QCS'02] D. Qiao, Sunghyun Choi, and Kang G. Shin, "*Goodput Analysis and Link Adaptation for IEEE 802.11a Wireless LANs*", IEEE Trans. on Mobile Computing, v.1, Nr.4, Oct-Dec 2002. p.p. 278-292.

[P'95] J. G. Proakis, Digital Communications. McGraw-Hill, New York, NY, USA, 3rd edition 1995.

[PK'02] K. Pahlavan and P. Krishnamurthy, "*Principles of Wireless Networks - A Unified Approach*", Prentice Hall, 2002.

[PM'06] J.Proakis, D. Manolakis, Digital Signal Processing, Prentice Hall, 4th edition, 2006.

[PTC'05] S. U. Pillai, T.Suel, and S.Cha, "*The Perron-Frobenius Theorem, some of its applacations*", IEEE Signal Processing Magazine, v.75, March 2005.

[R'02] T. S. Rappaport, Wireless Communications: Principles & Practice, Prentice Hall, 2nd Edition, 2002.

[RM'99] V. Rodoplu and T. H. Meng, "*Minimum energy mobile wireless networks*," IEEE J. Selected Areas in Communications, vol. 17, no. 8, August 1999.

[RPDGK'05] J. Robinson, K. Papagiannaki, C. Diot, X. Guo, and L. Krishnamurthy, "*Experimenting with a Multi-Radio Mesh Networking Testbed*", 1st workshop on Wireless Network Measurements (WiNMee 2005), Italy, Apr. 2005.

[RRH'00] R. Ramanathan and R. Rosales-Hain, "*Topology control of multihop wireless networks using transmit power adjustment*," in Proc. IEEE Infocom 2000, March 2000.

[RS'08] Rohde & Schwarz, FSH6 Handheld Spectrum Analyzer data sheet, online at: http://www2.rohde-schwarz.com/file/FSH_dat_en.pdf

[SW'08] Seattle Wireless, online at: http://www.seattlewireless.net/

[T'05] S. Toumpis, "*Distributed Power Control*", lecture slides, available online at: http://www.eng.ucy.ac.cy/toumpis/courses/ad_hoc/power_control.pdf

[TG'03] S.Toumpis, A. Goldsmith"*Capacity Regions for Ad hoc Networks*", Transactions on Wireless Communications, Vol. 2, No. 4, July 2003

[U'08] Ubiquiti SRC 802.11a/b/g datasheet, online at: http://ubnt.com/downloads/src_datasheet.pdf

[UY'98] S. Ulukus and R. Yates "*Stochastic Power Control for Cellular Radio Systems*", IEEE Transactions on Communications, vol. 46, No. 6, pp. 784-798, June 1998.

[VS'08] Vesuvius Streamline Antennas, online at: http://www.vesuviustreamline.com/

[W'98] J. Walrand, Communication Networks: A First Course, Second Edition, McGraw-Hill, New York, NY, USA, 1998

[W'08] Wikipedia: *List of wireless community networks by region*, available online at http://en.wikipedia.org/wiki/List_of_wireless_community_networks_by_region

[Y'95] R. Yates "*A Framework for Uplink Power Control in Cellular Radio Systems*" IEEE Journal on Selected Areas in Communications, vol. 13, No. 7, pp. 1341-1348, Sept. 1995.

[Za'92a] J. Zander, "*Distributed cochannel interference control in cellular radio systems*" IEEE Trans. Veh.Technol, vol. 41, no. 3, pp. 305–311, Aug. 1992.

[Za'92b] J. Zander, "*Performance of Optimum Transmitter Power Control in Cellular Radio Systems*", IEEE Transactions on Vehicular Technology, v41,no. 1, pp. 57-62, February 1992.

[Zi'80] H. Zimmermann, "*OSI Reference Model - The ISO Model of Architecture for Open Systems Interconnection*", IEEE Transactions on Communications COM-28, No. 4: April 1980.

[ZINK'07] M. Zink, T.Ireland, A.Nyzio, J. Kurose, "*The Impact of Directional Antenna Orientation, Spacing, and Channel Separation on Long-distance Multi-hop 802.11g Networks: A Measurement Study*", WiNMee 2007, Limassol, Cyprus, Apr. 2007.